Biointerface Research in Applied Chemistry
Open-Access Journal (ISSN: 2069-5837)

Article
Volume 16, Issue 1, 2026, 27
https://doi.org/10.33263/BRIAC161.027

New Thiadiazole and Benzothiazole Affixed Pyrazoles: Synthesis, Characterization, and Pharmacological Evaluation

Manjunatha C Ramegowda [1], Srikantamurthy Ningaiah [2], Vrushabendra Basavanna [2], Manasa Chandramouli [2], Nanjundaswamy G Siddamallappa [3], Shanthappa Nanjunda Swamy [4], Umesha K Bhadraiah [1,*]

[1] Department of Chemistry, Yuvaraja's College, University of Mysore, Mysuru, Karnataka, India–570005; sirichemresearcher@gmail.com (M.C.R.); drkbumesha@gmail.com (U.K.B.);
[2] Department of Chemistry, Vidyavardhaka College of Engineering, Visvesvaraya Technological University, Mysuru, Karnataka, India–570002; srijmn@vvce.ac.in (S.N.); vrushabendra@vvce.ac.in (V.B.); manasac@vvce.ac.in (M.C.);
[3] Department of Chemistry, The National Institute of Engineering, Mysuru, Karnataka, India–570018; nanjundaswamyogi@gmail.com (N.G.S.);
[4] Department of Chemistry, SJCE, JSS Science and Technology University, Mysuru-570006; nswamychem007@gmail.com (S.N.S.);
* Correspondence: drkbumesha@gmail.com;

Received: 5.08.2025; Accepted: 17.12.2025; Published: 15.02.2026

Abstract: A novel class of hybrid compounds, such as thiadiazolyl-pyrazoles (**14a-e**) and benzothiazolyl-pyrazoles (**15a-d**), has been successfully synthesized *via* a simple condensation reaction. Newly synthesized compounds have been characterized by mass, ^{1}H, and ^{13}C NMR spectral analysis. The target compounds have been studied for their DFT docking, antibacterial, antioxidant, and cytotoxicity properties. Among the target compounds, heterocycle **14e** showed significant binding with *penicillin G acyl-Penicillin* (1MWT) and *Escherichia coli DNA gyrase B* (6KZX) protein target, with binding scores -6.5 and -8.2 kcal/mol, respectively. In addition, the compounds **14c** and **14e** showed superior activity against both the microbes at different concentrations, whereas compounds **14a** and **14e** showed excellent antioxidant activity at 100 µg/mL concentration. Among the selected compounds, heterocycle **14e** exhibited significant anticancer activity against both triple-negative breast cancer (MDA-MB-231) and oestrogen receptor-positive breast cancer (MCF-7) cell lines, with 68.49 and 57.38% of inhibition, respectively.

Keywords: pyrazole; thiadiazole; benzothiazole; docking studies; antimicrobial; anticancer.

1. Introduction

Heterocycles have been reported in both commercial medications and drug discovery targets. Nitrogen-containing rings are particularly significant in the development of new drugs due to their diverse therapeutic and pharmacological activities [1]. Pyrazoles and their derivatives have significant interest due to their diverse biological actions, and the pyrazole ring is a crucial structural component in a number of marketed medications [2]. Certain pyrazole derivatives showed cytotoxicity in numerous human cell lines [3,4]. These are licensed for the treatment of various cancers, such as crizotinib (pyrazole-pyridine analog),

ruxolitinib (pyrazole-pyrrolo[2,3-*d*]pyrimidine analog), and erdafitinib (pyrazole-quinoxaline analog), which have already been approved for cancer therapy [5]. In the previous three decades (between 1990 and 2021), 50% deaths decreased among children and 80% increased among adults and older adults due to AMR, and 1.27 million deaths were caused all over the world in 2019. In the coming year 2050, researchers estimated the deaths of ten million people by AMR [6]. Norfloxacin, Amoxicillin, Ciprofloxacin, and Chloramphenicol are the most common drugs used for bacterial infections, but are linked with serious side effects [7]. Pyrazole derivatives have been found to possess considerable biological activities, such as antimicrobial, anti-inflammatory [8], anticancer [9], antiamoebic [10], antinociceptive [11], antidepressant [12], anti-fungal [13], antihypertensive [14], anti-HIV [15], and anticonvulsant activities [16]. Thus, heterocyclic derivatives containing the pyrazole moiety seem to be a possible pharmacophore in various pharmacologically active agents. We have found a few drugs, such as Remifenazone (Figure 1A), Butazolidine (Figure 1B), Mepirizole (Figure 1C), Antipyrazine (Figure 1D), and Celecoxib (Figure 1E), containing the same pyrazole moiety in core structure, and hence we planned to incorporate the pyrazole heterocycle with 1,3,4-thiadiazole and benzothiazole moieties.

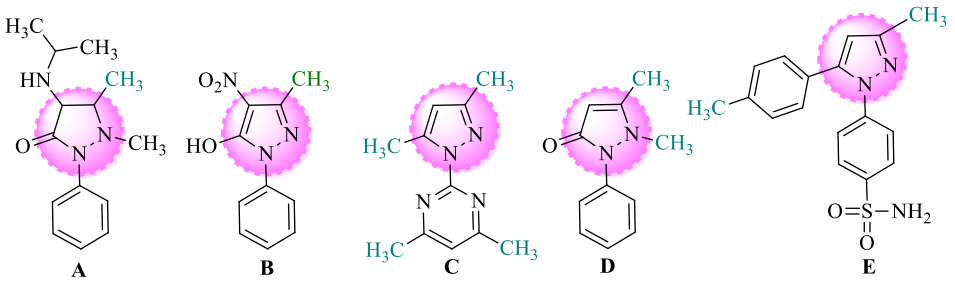

Figure 1. Biologically active compounds containing a pyrazole nucleus.

Thiadiazole derivatives are significant five-membered heterocyclic compounds in medicinal chemistry, valued for their stability and diverse pharmacological uses [17]. Modifications to the thiadiazole ring with various functional groups can enhance their biological potential, leading to potent and less toxic drug candidates [18]. Research highlights their robust anticancer and antitumor effects, often involving mechanisms such as inducing apoptosis and inhibiting cancer cell enzymes [19]. Studies also document their efficacy as antimicrobial, anti-inflammatory, and antiviral agents against targets including multidrug-resistant bacteria and HIV. Further therapeutic explorations include applications as antidiabetic, anticonvulsant, and antileishmanial agents, underscoring the thiadiazole scaffold's versatility in drug development [20]. Benzothiazole is a privileged bicyclic heterocyclic scaffold, formed by the fusion of a benzene ring and a five-membered thiazole ring containing nitrogen and sulfur atoms [21]. This unique structure is widely prevalent in natural products and synthetic therapeutic agents, making it a critical framework in modern medicinal chemistry. Derivatives of benzothiazole exhibit remarkable structural diversity, which allows them to interact with a broad array of biological targets and display a wide range of pharmacological activities [22]. Notable applications include significant anticancer properties, as they can target various cellular processes and receptors, such as kinases and tubulin polymerization [23]. They also serve as potent antimicrobial agents against bacteria, fungi, and viruses [24], including drug-resistant strains. Furthermore, benzothiazole derivatives are developed as effective anti-inflammatory, antidiabetic [25], and neuroprotective agents. Clinically approved drugs such as the ALS treatment riluzole [26], the Parkinson's disease

medication pramipexole [27], and the Alzheimer's disease imaging agent flutemetamol [28] all incorporate the benzothiazole core, demonstrating its substantial therapeutic potential.

Another class of biologically significant compounds with pharmaceutical applications is Schiff bases. These compounds, also known as imines or azomethines, are formed by condensation of primary amines with aldehydes or ketones, a reaction first described by Hugo Schiff in 1864 [29, 30]. Bifunctional Schiff bases have been the subject of considerable investigation due to their structural diversity and ease of synthesis, making them valuable as intermediates in organic synthesis, as luminescent chemosensors, for corrosion inhibition, and for polymer stabilization [31]. Furthermore, Schiff bases exhibit a broad spectrum of pharmacological activities, including anticancer, antioxidant, antifungal, antibacterial, anti-inflammatory, antiviral [32], antimalarial, anti-HIV, and antipyretic properties [33], and the presence of the azomethine bond is believed to be essential for biological activity [34].

In addition, hybrid compounds containing pyrazole, thiadiazole, and benzothiozole have been reported as a potent scaffold for Pyrazole–Thiadiazole-based inhibitors that showed inhibitor activity against the human cell line [35], antifungal activity [36], herbicidal activity [36], and antitumor activity [37]. The pyrazole–benzothiazole–based compound showed antiproliferative [38], antimicrobial, antioxidant, anti-TB activities [39], and antibacterial and antifungal activities [40].

The above observations motivated us to synthesize bifunctional heterocycles linked *via* an imine bond, with the aim of targeting pharmacological activities.

2. Materials and Methods

2.1. Chemistry.

The Bruker AV400 spectrometer was used to obtain the ^{1}H NMR ($CDCl_3$) at 400 MHz and ^{13}C NMR ($CDCl_3$) spectra at 100 MHz, respectively. δ ppm is used to express chemical shift values. Joel's JMS-D-300 mass spectrometer was used to obtain the mass spectra of synthesized compounds. Thin-layer chromatography (TLC) was used to monitor each reaction's progress, and column chromatography was used to purify **14(a-e)** and **15(a-d)** compounds. All analytical grade reagents (AR) were used throughout the synthesis.

2.1.1. Synthesis of pyrazole carboxaldehydes (4 and 7).

The method used for the synthesis of pyrazole derivatives is depicted in Scheme 1. Pyrazole derivative (**3**) was synthesized by treating acetyl acetone (**2**, 0.204 g, 1 mmol) with phenyl hydrazine (**1**, 0.218 g, 1 mmol) under reflux conditions at 70°C using the reported method [41]. NMR spectral analyses are provided in the supporting information (Figures S1 and S2). 3,5-dimethyl-1-phenyl-1*H*-pyrazole-4-carbaldehyde (**4**) was synthesized by treating compound (**3**) with phosphorus oxychloride ($POCl_3$) in DMF (4 mL) using a previously reported method [42]. Subsequently, ethylacetoacetate (**5**, 5 g, 4.9 mL, 0.384 mol) was treated with phenyl hydrazine (**1**, 4 g, 3.65 mL, 0.37 mol) in the presence of a few drops of acetic acid to yield pyrazolone (**6**) [43]. In the later step, 5-chloro-3-methyl-1-phenyl-1*H*-pyrazole-4-carbaldehyde (**7**) was synthesized by treating previously obtained compound **6 (**4 g, 0.025 mol) with $POCl_3$ (16.0 mL, 0.17 mol) and DMF (6.0 mL, 0.8 mol) at 0°C [44].

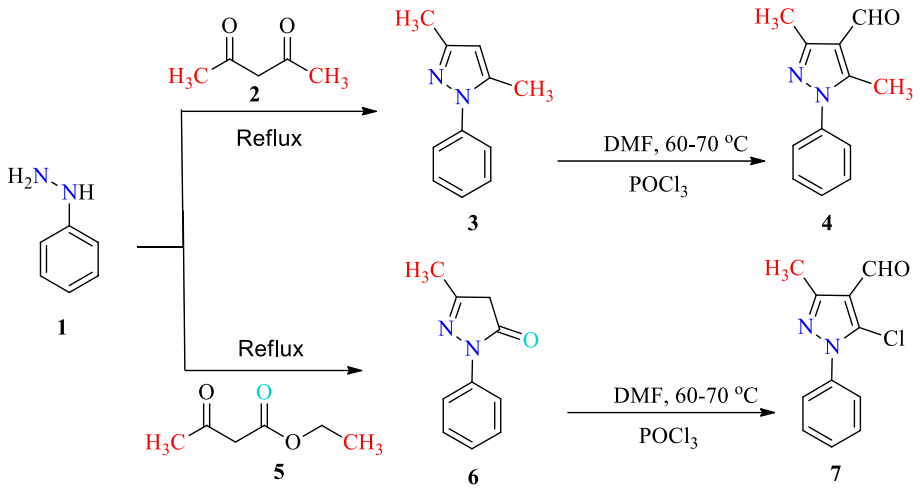

Scheme 1. Synthesis of 3,5-dimethyl-1-phenyl-1*H*-pyrazole-4-carbaldehyde (**4**) and 5-chloro-3-methyl-1-phenyl-1*H*-pyrazole-4-carbaldehyde (**7**).

2.1.2. Synthesis of 5-phenyl-1,3,4-thiadiazol-2-amine (10a) and 2-amino-4-methylbenzothiazole (12a).

Benzoic acid (**8a**, 1.34 g, 10.9 mmol) and thiosemicarbazide (**9**, 1 g, 10.9 mmol) were dissolved in phosphorus oxychloride (10.25 mL, 109.7 mol) and gently refluxed for 40 minutes. The reaction mixture was cooled, followed by careful addition of ice-cold water drop by drop, and the resulting precipitate was collected after basification with saturated KOH. The solid was purified by recrystallization from DMF-EtOH (9:1) to yield compound **10a**, as previously reported in the literature [45]. Following the same procedure, the compounds **10(b-e)** were synthesized (Scheme 2), and the LC-MS spectral analysis of compound **10(a-c)** was supported by supporting information (Figure S3-S7).

A mixture of 4-methylaniline (**11a**, 1 g, 9.3 mmol) and potassium thiocyanate (**13**, 0.99 g, 10.0 mmol) in acetic acid (37 mL) was stirred for 30 minutes, followed by the addition of a solution of bromine (0.48 mL, 10.0 mmol) in acetic acid, which was added dropwise over 30-35°C. The resulting slurry was swirled at room temperature, and the precipitate of 2-amino-4-methylbenzothiazole (**12a)** was filtered, washed with ammonia solution and finally with water. After that, the crude solid was recrystallized from aqueous ethanol. Followed, the same procedure [46] is used to synthesize **12(b-d)** (Scheme 2).

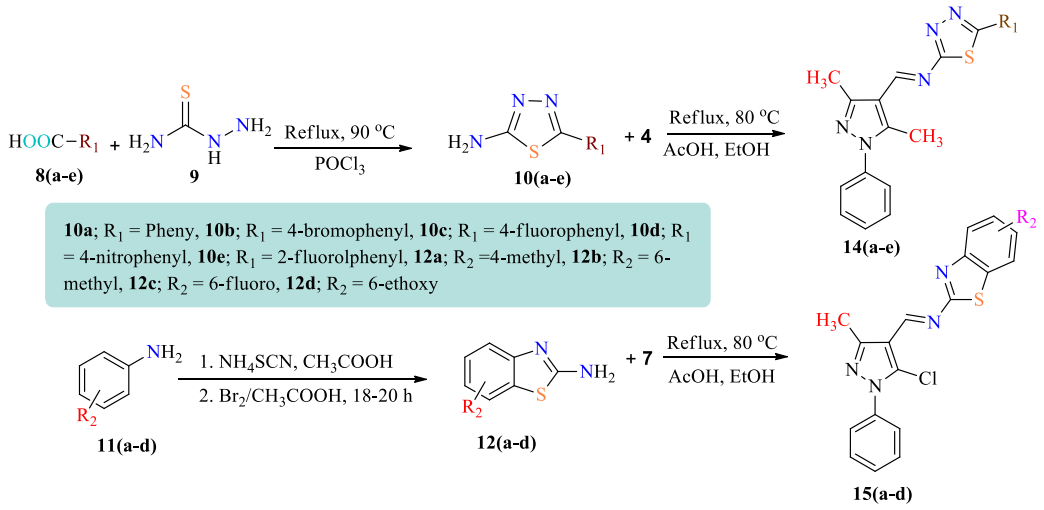

Scheme 2. General scheme for the synthesis of substituted thiadiazole and benzothiazole amine derivatives.

2.1.3. Synthesis of (*E*)-*N*-((3,5-dimethyl-1-phenyl-1*H*-pyrazol-4-yl)methylene)-5-phenyl-1,3,4-thiadiazol-2-amine (14a).

A mixture of 3,5-dimethyl-1-phenyl-1*H*-pyrazole-4-carbaldehyde (**4**, 0.140 g, 0.69 mmol) and 5-phenyl-1,3,4-thiadiazol-2-amine (**10a**, 0.123 g, 0.69 mmol) was added to a clean 25 mL round-bottom flask containing 15 mL of dry ethanol and glacial acetic acid (0.420g, 6.9 mmol). The reaction mixture was refluxed for 14 hours at 80°C, and the progress was monitored using thin-layer chromatography (TLC) (hexane/ethyl acetate, 7:3). After completion, the reaction mixture was cooled to room temperature, and the precipitated product was filtered to obtain the target compound **14a**. The compound was further purified by recrystallization from ethanol and by column chromatography. ^{1}H NMR, ^{13}C NMR, FTIR and MS spectral analysis of compound **10(a-c)** proved by supporting information's (Figure S8-S29).Yield: 91% (0.228 g, yellow colour); IR (ν, cm^{-1}): 1619 (-CH=N-), 1596 (C=C), 1560 (C=N), 691 (C-S); ^{1}H NMR ($CDCl_3$, 400 MHz): δ = 9.97 (s, CH=N, 1H), 7.55–7.45 (m, Ar-H, 9H), 2.53 (s, $2CH_3$, 6H); ^{13}C NMR ($CDCl_3$, 100 MHz, δ ppm): 183.89, 161.30, 152.71, 151.80, 138.31, 137.66, 136.99, 129.30, 129.30, 129.22, 129.20, 128.91, 126.57, 125.21, 124.49, 121.12, 117.44, 109.53, 13.84, 12.92; MS (m/z): 359.45; Anal. Calcd. for $C_{20}H_{17}N_5S$: C, 66.85; H, 4.73; N, 19.49; Found: C, 66.66; H, 4.72; N, 19.44%. This method was used to synthesize all the target compounds **14(b-e)** and **15(a-d)** (Scheme 2).

2.1.4. (5-(4-bromophenyl)-*N*-((3,5-dimethyl-1-phenyl-1*H*-pyrazol-4-yl)methylene)-1,3,4-thiadiazol-2-amine (14b).

Obtained from the reaction of 3,5-dimethyl-1-phenyl-1*H*-pyrazole-4-carbaldehyde (**4**, 0.140 g, 0.69 mmol), 5-(4-bromophenyl)-1,3,4-thiadiazol-2-amine (**10b**, 0.179 g, 0.69 mmol). Yield: 83% (0.249 g, brown colour); IR (ν, cm^{-1}): 1615 (-CH=N-), 1598 (C=C), 1564 (C=N), 1060 (C-Br), 696 (C-S); ^{1}H NMR ($CDCl_3$, 400 MHz): δ = 9.03 (s, CH=N, 1H), 7.86–7.48 (m, Ar-H, 9H), 2.65-2.59 (s, $2CH_3$, 6H). ^{13}C NMR ($CDCl_3$, 100 MHz, δ ppm): 175.42, 165.24, 159.67, 152.11, 144.37, 138.42, 132.34, 132.33, 132.20, 129.78, 129.37, 129.36, 128.83, 128.74, 125.34, 125.20, 115.98, 29.70, 13.14, 12.21; MS (m/z): 439.45; Anal. Calcd. for $C_{20}H_{16}N_5S$: C, 54.79; H, 3.65; N, 15.98; Found: C, 54.61; H, 3.64; N, 15.92%.

2.1.5. *N*-((3,5-dimethyl-1-phenyl-1*H*-pyrazol-4-yl)methylene)-5-(4-fluorophenyl)-1,3,4-thiadiazol-2-amine (14c).

Obtained from the 3,5-dimethyl-1-phenyl-1*H*-pyrazole-4-carbaldehyde (**4**, 0.140 g, 0.69 mmol), 5-(4-fluorophenyl)-1,3,4-thiadiazol-2-amine (**10c**, 0.136 g, 0.69 mmol). Yield: 94% (0.247 g, White colour); IR (ν, cm^{-1}): 1624 (-CH=N-), 1603 (C=C), 1567 (C=N), 1260 (C-F), 698 (C-S); ^{1}H NMR ($CDCl_3$, 400 MHz): δ = 9.03 (s, CH=N, 1H), 7.99–7.20 (m, Ar-H, 9H), 2.65 (s, CH_3, 3H), 2.59 (s, CH_3, 3H). ^{13}C NMR ($CDCl_3$, 100 MHz, δ ppm): 175.24, 165.50, 165.20, 163.00, 159.58, 152.07, 144.32, 138.42, 129.50, 129.42, 129.37, 128.73, 127.13, 125.34, 116.41, 116.19, 116.03, 115.96, 13.15, 12.22; MS (m/z): 378.19; Anal. Calcd. for $C_{20}H_{16}FN_5S$: C, 63.46; H, 4.24; N, 18.56; Found: C, 63.46; H, 4.23; N, 18.50%.

2.1.6. *N*-((3,5-dimethyl-1-phenyl-1*H*-pyrazol-4-yl)methylene)-5-(4-nitrophenyl)-1,3,4-thiadiazol-2-amine (14d).

Obtained from the 3,5-dimethyl-1-phenyl-1*H*-pyrazole-4-carbaldehyde (**4**, 0.140 g, 0.69 mmol), 5-(4-nitrophenyl)-1,3,4-thiadiazol-2-amine (**10d**, 0.155 g, 0.69 mmol). Yield:

44% (0.124 g, brown colour); IR (ν, cm^{-1}): 1625 (-CH=N-), 1601 (C=C), 1564 (C=N), 1345 (C-NO_2), 693 (C-S); ^{1}H NMR ($CDCl_3$, 400 MHz): δ = 9.03 (s, CH=N, 1H), 8.38–7.46 (m, Ar-H, 9H), 2.66 (s, CH_3, 3H), 2.55 (s, CH_3, 3H). ^{13}C NMR ($CDCl_3$, 100 MHz, δ ppm): 175.42, 165.24, 159.67, 152.11, 144.37, 139.7, 138.42, 132.34, 129.78, 129.37, 129.30, 128.83, 128.74, 125.34, 125.30, 125.20, 115.98, 29.70, 13.14, 12.21; MS (m/z): 405.53; Anal. Calcd. for $C_{20}H_{16}N_6O_2S$: C, 59.38; H, 3.95; N, 20.78; Found: C, 59.18; H, 3.94; N, 20.71%.

2.1.7. *N*-((3,5-dimethyl-1-phenyl-1*H*-pyrazol-4-yl)methylene)-5-(2-fluorophenyl)-1,3,4-thiadiazol-2-amine (14e).

Obtained from the 3,5-dimethyl-1-phenyl-1*H*-pyrazole-4-carbaldehyde (**4**, 0.140 g, 0.69 mmol), 5-(2-fluorophenyl)-1,3,4-thiadiazol-2-amine (**10e**, 0.136 g, 0.69 mmol). Yield: 87% (0.228 g, white colour); IR (ν, cm^{-1}): 1620 (-CH=N-), 1598 (C=C), 1567 (C=N), 1263 (C-F), 696 (C-S); ^{1}H NMR ($CDCl_3$, 400 MHz): δ = 10.01 (s, CH=N, 1H), 7.59–7.49 (m, Ar-H, 9H), 2.59 (s, CH_3, 3H), 2.57 (s, CH_3, 3H). ^{13}C NMR ($CDCl_3$, 100 MHz, δ ppm): 184.00, 161.38, 152.80, 151.89, 138.42, 137.73, 137.06, 133.58, 129.39, 129.33, 129.31, 129.00, 126.66, 125.30, 125.27, 121.22, 117.51, 109.62, 13.93, 13.02; MS (m/z): 378.53; Anal. Calcd. for $C_{20}H_{16}FN_5S$: C, 63.64; H, 4.24; N, 18.56; Found: C, 63.40; H, 4.22; N, 18.49%.

2.1.8. *N*-((5-chloro-3-methyl-1-phenyl-1*H*-pyrazol-4-yl)methylene)-4-methylbenzo[d]thiazol-2-amine (15a).

Obtained from the 5-chloro-3-methyl-1-phenyl-1*H*-pyrazole-4-carbaldehyde (**7**, 0.100 g, 0.45 mmol), 4-methylbenzo[*d*]thiazol-2-amine (**12a**, 0.073 g, 0.45 mmol). Yield: 89% (0.145 g, brown colour); IR (ν, cm^{-1}): 1623 (-CH=N-), 1595 (C=C), 1560 (C=N), 763 (C-Cl), 698 (C-S); ^{1}H NMR ($CDCl_3$, 400 MHz): δ = 10.01 (s, CH=N, 1H), 7.57–7.53 (m, Ar-H, 8H), 2.57 (s, 2CH_3, 6H); ^{13}C NMR ($CDCl_3$, 100 MHz, δ ppm): 175.43, 165.23, 159.70, 152.12, 144.39, 138.41, 135.02, 133.30, 132.35, 129.77, 129.39, 128.83, 128.75, 126.62, 125.34, 125.21, 115.98, 13.18, 12.24; MS (m/z): 367.49; Anal. Calcd. for $C_{19}H_{15}ClN_4S$: C, 62.28; H, 4.09; N, 15.29; Found: C, 62.04; H, 4.08; N, 15.23%.

2.1.9. *N*-((5-chloro-3-methyl-1-phenyl-1*H*-pyrazol-4-yl)methylene)-6-methylbenzo[d]thiazol-2-amine (15b).

Obtained from the 5-chloro-3-methyl-1-phenyl-1*H*-pyrazole-4-carbaldehyde (**7**, 0.100 g, 0.45 mmol) and 6-methylbenzo[*d*]thiazol-2-amine (**12b**, 0.074 g, 0.45 mmol). Yield: 63% (0.100 g, brown colour); IR (ν, cm^{-1}): 1622 (-CH=N-), 1600 (C=C), 1565 (C=N), 765 (C-Cl), 696 (C-S); ^{1}H NMR ($CDCl_3$, 400 MHz): δ = 10.00 (s, CH=N, 1H), 7.58–7.44 (m, Ar-H, 8H), 2.53 (s, 2 x -CH_3, 6H); ^{13}C NMR ($CDCl_3$, 100 MHz, δ ppm): 175.41, 165.19, 159.74, 152.10, 144.41, 138.43, 136.22, 132.33, 130.20, 129.75, 129.37, 128.80, 128.75, 125.31, 125.20, 124.80, 115.99, 13.16, 12.21; MS (m/z): 366.06; Anal. Calcd. for $C_{19}H_{15}ClN_4S$: C, 62.28; H, 4.09; N, 15.29; Found: C, 62.28; H, 4.09; N, 15.29%.

2.1.10. (*N*-((5-chloro-3-methyl-1-phenyl-1*H*-pyrazol-4-yl)methylene)-7-fluorobenzo[d] thiazol-2-amine (15c).

Obtained from the 5-chloro-3-methyl-1-phenyl-1*H*-pyrazole-4-carbaldehyde (**7**, 0.100 g, 0.45 mmol) and 7-fluorobenzo[*d*]thiazol-2-amine (**12c**, 0.076 g, 0.45 mmol). Yield: 51% (0.085 g, pale yellow colour); IR (ν, cm^{-1}): 1621 (-CH=N-), 1598 (C=C), 1566 (C=N), 768 (C-

Cl), 695 (C-S); ^{1}H NMR ($CDCl_3$, 400 MHz): δ = 10.00 (s, CH=N, 1H), 7.93–7.29 (m, Ar-H, 8H), 2.20 (s, -CH_3, 3H), 2.19 (s, -CH_3, 3H); ^{13}C NMR ($CDCl_3$, 100 MHz, δ ppm): 174.6, 160.0, 154.8, 149.2, 140.4, 137.2, 136.7, 133.3, 129.3, 129.3, 127.6, 126.2, 124.8, 124.8, 117.4, 114.6, 113.9, 13.7; MS (m/z): 370.05; Anal. Calcd. for $C_{18}H_{12}ClFN_4S$: C, 58.37; H, 3.24; N, 15.13; Found: C, 58.37; H, 3.24; N, 15.13%.

2.1.11. *N*-((5-chloro-3-methyl-1-phenyl-1*H*-pyrazol-4-yl)methylene)-6-ethoxybenzo[d] thiazol-2-amine (15d).

Obtained from the 5-chloro-3-methyl-1-phenyl-1*H*-pyrazole-4-carbaldehyde (**7**, 0.100 g, 0.45 mmol) and 6-ethoxybenzo[*d*]thiazol-2-amine (**12d**, 0.088 g, 0.45 mmol). Yield: 88% (0.158 g, salmon colour); IR (ν, cm^{-1}): 1674 (-CH=N-), 1597 (C=C), 1525 (C=N), 1004 (C-O), 762 (C-Cl), 696 (C-S); ^{1}H NMR ($CDCl_3$, 400 MHz): δ = 8.98 (s, CH=N, 1H), 7.88–7.06 (m, Ar-H, 8H), 4.15 (q, -OCH_2-, 2H), 2.71 (s, -CH_3, 3H), 1.50 (t, -CH_3, 3H); ^{13}C NMR ($CDCl_3$, 100 MHz, δ ppm): 170.07, 156.93, 156.29, 151.80, 146.08, 137.35, 135.59, 132.22, 129.25, 128.96, 125.03, 124.80, 123.56, 115.91, 115.22, 105.19, 64.11, 29.71, 14.96, 14.86; MS (m/z): 398.13; Anal. Calcd. for $C_{20}H_{17}ClN_4OS$: C, 60.59; H, 4.29; N, 14.13; Found: C, 60.28; H, 4.26; N, 14.06%.

2.2. Biology and molecular docking studies.

2.2.1. ADMET studies.

Two Important computational web-based applications, SwissADME and pkCSM, were used to systematically evaluate the pharmacokinetic properties and drug-likeness profiles of the synthesized compounds. These tools provide a quick and effective method for predicting important ADMET (Absorption, Distribution, Metabolism, Excretion, and Toxicity) parameters in the initial stages of drug discovery. Drug-likeness parameters, such as the boiled-egg model and the bioavailability radar, visually represent the pharmacokinetic behaviour of substances. It further carefully examined if the compounds satisfied standard drug-likeness rules, such as the Lipinski, Ghose, Veber, Egan, and Muegge filters. Initially, the SMILES (Simplified Molecular-Input Line-Entry System) notation was generated from the chemical structures of the compounds using ChemDraw Professional 16.0.1.4 (77) software. The pkCSM and SwissADME tools were then used to predict and analyze the compound's pharmacokinetic and drug-likeness properties using these SMILES strings as input [47, 48].

2.2.2. Molecular docking studies.

Using AutoDock Vina, molecular docking was performed to determine the binding affinity of the protein-ligand complexes, with binding energies reported in kcal/mol. The docking process includes developing a grid box that completely covers the target protein's active site, with grid dimensions set to (x=40, y=40, z=40) and the grid center coordinates placed at (x=-1.7890, y=37.6273, z=66.2371 and x=27.582, y=5.2871, z=-8.073 of PDB ID:1MWT and 6KZX respectively). The virtual molecular docking was carried out using AutoDock Vina version 1.5.7. Biovia Discovery Studio Visualizer 2021 was used to visualize and analyze protein-ligand interactions, showing each ligand accurately docked into the designated active site of the protein (1MWT, 6KZX). The compounds with the strongest

interactions with the target protein were those with favorable binding scores, as indicated by the lowest (most negative) binding energies [49].

2.2.3. In vitro antibacterial screening.

The antibacterial screening for newly prepared compounds was determined by the disc diffusion method [50] using Mueller–Hinton Agar (MHA) medium. The synthesized compounds were evaluated against Gram-negative bacteria of *E. coli* and Gram-positive bacteria of *S. aureus*. Synthesized compounds were initially screened at different concentrations (50, 40, 30, 20, and 10 µg/mL) in DMSO. The zone of inhibition was measured after 24h incubation at 37°C [51]. Antibiotic discs ampicillin (5 µg/mL) and ciprofloxacin (10 µg/mL) were used as positive controls for *S. aureus* and *E. coli*. Experiments were performed in triplicate (n = 3), and values given are the mean of triplicates ± standard error.

2.3. Antioxidant activity.

2.3.1. DPPH (2,2-diphenyl-1-picrylhydrazyl) radical scavenging assay.

The DPPH radical scavenging activity of the synthesized compounds was evaluated following the method described by Aksoy *et al*. [52]. In this *in vitro* assay, a 140 µL solution of DPPH (6.2 mg dissolved in 100 mL ethanol) was incubated with varying concentrations of the test compounds for 30 minutes in the dark. It is based on the reduction of the stable DPPH radical to its non-radical form (DPPH-H) upon interaction with an antioxidant, resulting in a decrease in absorbance at 536 nm measured with a UV-visible spectrophotometer. Vitamin C was used as the standard antioxidant for comparison (Supporting information Table S3.1-S3.10).

The percentage of free radical scavenging activity (%RSA) was calculated using the following formula:

$$\text{DPPH radical scavenging activity} = \frac{[A_o - A_1]}{A_o} \times 100 \qquad (1)$$

Where: A_0 = Optical density (OD) of the DPPH solution incubated with solvent (blank control). And A_1 = OD of the DPPH solution incubated with the test compound [53].

2.3.2. Ferric reducing antioxidant power (FRAP) assay.

The FRAP assay was conducted according to the method outlined by Benzie *et al*. [54] (1999). This method measures the reduction of the ferric-tripyridyltriazine (Fe^{3+}-TPTZ) complex to the ferrous form (Fe^{2+}-TPTZ), which results in the formation of a blue-colored complex with an absorbance maximum at 593 nm. The FRAP reagent containing 2.5mL of 10mM TPTZ (2,4,6- trypyridyl-s-triazine), 2.5mL of 20mM $FeCl_3$ and 25mL of 300mM acetate buffer, pH = 3.6, was prepared by warming at 37°C. 190µL FRAP reagent was incubated with a suitably diluted solution by total phenol content and $FeSO_4$ (standard: 200-1800µM) in the dark for 30 min, and the absorbance was measured at 593 nm (Supporting information Table S4.1-S4.8). FRAP units (equivalent amount of ferrous sulfate) were calculated, and the data are plotted against the concentration of extract. All antioxidant assays were performed in triplicate, and the results are presented as mean ± standard error (SE) [55]. Reference sample was prepared (ascorbic acid, 1 mg/mL) [56].

2.4. Cytotoxicity.

2.4.1. Cytotoxicity against breast cancer cell lines.

Cell viability assessment using Sulforhodamine B (SRB) Assay. The cytotoxic potential of the synthesized compounds was evaluated using the Sulforhodamine B (SRB) assay, which quantifies cell viability based on the ability of SRB dye to bind to basic amino acid residues in trichloroacetic acid (TCA)-fixed cells in a pH-dependent manner.

2.4.2. Cell culture and treatment.

Human breast cancer cell lines, MCF-7 (ER/PR-positive) and MDA-MB-231 (ER/PR/HER2-negative), were utilized for the cytotoxicity assay. Cells were seeded at a density of 1×10^4 cells/well in a 96-well plate containing DMEM supplemented (Dulbecco's modified Eagle's medium) with 10% fetal bovine serum (FBS) and incubated at 37°C in a CO_2 incubator for 36 hours [57]. After reaching the exponential growth phase, cells were treated with increasing concentrations of the compounds **14a**, **14c**, **14d**, **14e**, **15c**, and **15d**, 200 µM *cisplatin* (positive control), and 1% DMSO (vehicle control). The compounds **14a**, **14c**, **14d**, **14e**, **15c**, and **15d** were dissolved in dimethyl sulfoxide (DMSO) to achieve a stock concentration of 5 mM and subsequently stored at -20°C for 5 days before use. For cell culture treatments, the 5 mM stock solutions were diluted to final concentrations of 1 µM, 500 µM, and 1000 µM using respective supplemented cell culture media. The percentage inhibition (%I) was determined after 48 hours of exposure. Cell viability was assessed by SRB staining, and absorbance was measured to evaluate the cytotoxic effects of the test compounds.

3. Results and Discussion

3.1. Chemistry.

The synthesis method of novel pyrazole bearing thiadiazole and benzothiazole derivatives is shown in Scheme 2. The 3,5-dimethyl-1-phenyl-1*H*-pyrazole-4-carbaldehyde and 5-chloro-3-methyl-1-phenyl-1*H*-pyrazole-4-carbaldehyde (**7**) were synthesized by treating with phenyl hydrazine, acetyl acetone (**2**), and ethylacetoacetate (**5**) *via* the intermediates 3,5-dimethyl-1-phenyl-1*H*-pyrazole (**3**) and 3-methyl-1-phenyl-1*H*-pyrazol-5(4*H*)-one (**6**) by Vilsmeier reagent, respectively. The target compounds Schiff base-functionalized pyrazole-thiadiazole (**14a**–**e**) and pyrazole-benzothiazole (**15a**–**d**) were successfully synthesized by treating the pyrazole aldehydes **4** and **7** with thiadiazole amine (**10a-e**) and benzothiazole amine (**12a-d**) derivatives in ethanol as a solvent through a condensation reaction in the presence of acetic acid as a catalyst. The structures of all final compounds were confirmed by IR, NMR, and MS analyses. The appearance of molecular ion peaks at 378.19, 405.53, 366.04, 370.05, and 398.13 in mass spectra corresponding to their molecular mass indicated the formation of compounds **14c**, **14d**, **15b**, **15c**, and **15d**, respectively. In the IR spectra the appearance of absorption bands at 1619 cm^{-1}, 1596 cm^{-1}, 1560 cm^{-1} and 691 cm^{-1} corresponding to -CH=N-, -C=C-, -C=N- and -C-S stretching for **14a**, an absorption band 1674 cm^{-1}, 1597 cm^{-1}, 1525 cm^{-1}, 1004 cm^{-1}, 762 cm^{-1} and 696 cm^{-1} corresponding to -CH=N-, -C=C-, -C=N-, -C-O-, -C-Cl and -C-S- stretching for **15d** supported the structures of the corresponding final compounds. In the ^1H NMR spectra, the appearance of a singlet $\delta = 9.97$ due to the -CH=N- and a sharp singlet $\delta = 2.53$ due to $-CH_3$ groups and a singlet $\delta = 10.01$ due to the -CH=N-, a sharp singlet $\delta = 2.57$

due to CH_3 groups confirmed the structure of compounds **14a** and **15a**, respectively. In the ^{13}C NMR spectra, the appearance of a signal at δ = 13.14 and 12.21 due to the two-CH_3 group, and at δ = 161.30 due to the -CH=N- group. δ = 13.93 and13.02 due to the two -CH_3 groups, at δ = 161.38 due to the -CH=N- group supported the structure assigned to compounds **14a** and **15a**, respectively. The spectral study of all other derivatives also confirmed the structures assigned to the respective compounds.

3.2. ADMET and docking studies.

3.2.1. ADME and toxicity parameters.

In order to anticipate oral bioavailability and drug-like behavior, the given compounds (**14a**, **14c**, **14d**, **14e**, and **15d**) were evaluated for druglikeness using widely accepted pharmacokinetic and structural filters. This study shows that these compounds have good permeability and metabolism (see Table 1) and adhere to Lipinski's Rule of Five, with no violations (see Table 2). The compound's suitability as a possible drug candidate is further confirmed by its successful compatibility with the Ghose, Veber, Egan, and Muegge filters. The compounds have beneficial pharmacokinetic properties for further pharmaceutical research, as indicated by a bioavailability score of 0.55, suggesting a moderate probability of oral bioavailability. Since they meet important requirements for increasing bioavailability, absorption, and overall therapeutic efficacy, these properties collectively support the potential of the compounds **14a**, **14c**, **14d**, **14e**, and **15d** for drug development. The drug-likeness parameters, such as the boiled-egg model and bioavailability radar, which visually represent the pharmacokinetic behaviour of the substances, are shown in Figures 2, 3, and 4. The compounds show good intestinal absorption and moderate $CaCO_2$ permeability; water solubility is low across the series. Most molecules act as P-gp I/II inhibitors, aiding permeability but potentially causing drug–drug interactions. Distribution profiles indicate moderate VDss, limited BBB penetration for most, and all are CYP3A4 substrates with broad CYP inhibition tendencies. Toxicity results show no major hERG I risk, though some compounds exhibit AMES positivity and hepatotoxicity, requiring caution. Overall, compounds **14c** and **14d** appear more favorable in absorption.

Table 1. ADME and toxicity parameters results for target compounds.

Parameters	Model Name	14a	14b	14c	14d	14e	15a	15b	15c	15d
Absorption	Water solubility	-4.218	-4.48	-4.902	-4.584	-5.113	-5.589	-5.702	-5.593	-5.507
	$CaCO_2$ permeability	1.046	1.035	1.064	1.364	1.063	1.067	1.073	1.05	1.068
	Intestinal absorption (human)	95.856	94.272	96.386	100	95.531	94.757	94.901	94.203	94.956
	Skin permeability	-2.719	-2.718	-2.631	-2.733	-2.617	-2.557	-2.543	-2.62	-2.625
	P-glycoprotein substrate	No	No	No	No	No	No	No	Yes	No
	P-glycoprotein I inhibitor	Yes	Yes	Yes	Yes	Yes	No	Yes	Yes	Yes
	P-glycoprotein II inhibitor	Yes	Yes	Yes	Yes	Yes	Yes	Yes	Yes	Yes
Distribution	VDss (human)	0.245	0.341	0.222	0.084	0.086	0.35	0.309	-0.026	0.364
	Fraction unbound (human)	0.147	0.149	0.178	0.119	0.157	0.147	0.136	0.155	0.132
	BBB permeability	0.359	0.31	0.53	-1.178	0.571	0.449	0.467	0.309	0.192
	CNS permeability	-1.858	-1.717	-1.859	-2.028	-1.821	-1.323	-1.327	-1.334	-1.764
Metabolism	CYP2D6 substrate	No	No	No	No	No	No	No	No	No
	CYP3A4 substrate	Yes	Yes	Yes	Yes	Yes	Yes	Yes	Yes	Yes
	CYP1A2 inhibitor	Yes	Yes	Yes	Yes	Yes	Yes	Yes	Yes	Yes
	CYP2C19 inhibitor	Yes	Yes	Yes	Yes	Yes	Yes	Yes	Yes	Yes
	CYP2C9 inhibitor	Yes	Yes	Yes	Yes	Yes	Yes	Yes	Yes	Yes
	CYP2D6 inhibitor	No	No	No	No	No	No	No	No	No
	CYP3A4 inhibitor	Yes	Yes	Yes	Yes	Yes	Yes	Yes	No	Yes
Excretion	Total clearance	0.359	0.206	0.106	0.262	0.215	0.383	0.318	0.396	0.463
	Renal OCT2 substrate	Yes	Yes	Yes	No	Yes	Yes	Yes	No	Yes

Parameters	Model Name	14a	14b	14c	14d	14e	15a	15b	15c	15d
Toxicity	AMES toxicity	No	No	No	Yes	No	Yes	Yes	No	No
	Max. tolerated dose (human)	0.707	0.617	0.148	0.532	-0.108	-0.04	-0.197	-0.231	0.071
	hERG I inhibitor	No	No	No	No	No	No	No	No	No
	hERG II inhibitor	Yes	Yes	No	Yes	Yes	No	No	No	No
	Oral rat acute toxicity (LD_{50})	2.394	2.415	2.171	3.039	2.168	2.128	2.11	1.932	2.327
	Oral rat chronic toxicity (LOAEL)	0.843	0.66	0.99	0.785	1.021	0.864	0.992	0.713	0.882
	Hepatotoxicity	No	No	Yes	Yes	Yes	No	Yes	No	Yes
	Skin sensitisation	No	No	No	No	No	No	No	No	No
	T. pyriformis toxicity	0.294	0.295	0.323	0.288	0.355	0.451	0.519	0.541	0.377
	Minnow toxicity	-1.84	-2.655	-2.516	-3.236	-2.476	-2.385	-1.899	-1.729	-2.439

Table 2. Druglikeness results.

Druglikeness			
14a, **14c**, **14d**, **14e** and **15d** compounds		**15a**, **15b** and **15c** compounds	
Lipinski	Yes; 0 violations	Lipinski	Yes; 1 violation: MLOGP>4.15
Ghose	Yes	Ghose	Yes
Veber	Yes	Veber	Yes
Egan	Yes	Egan	Yes
Muegge	Yes	Muegge	No; 1 violation: XLOGP3>5
Bioavailability score	0.55	Bioavailability score	0.55

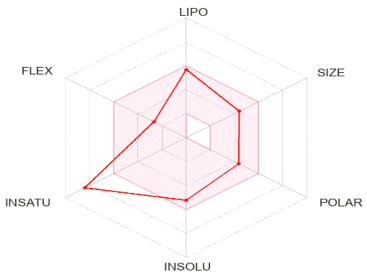

Figure 2. Bioavailability radar of 14a, 14c, 14d, 14e, and 15d.

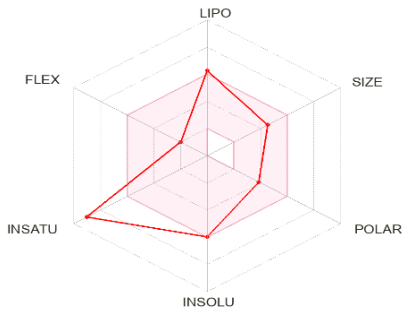

Figure 3. Bioavailability radar of 14b, 15a, 15b, and 15c.

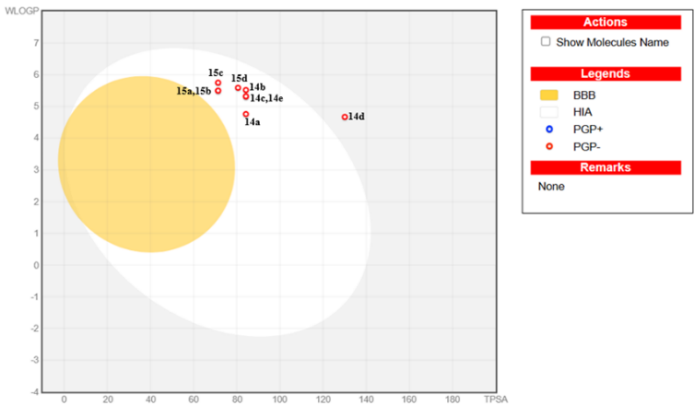

Figure 4. Boiled-egg model of compounds of **14(a-e)** and **15(a-d).**

3.2.2. Druglikeness studies by using the Swiss-ADME tool.

In order to determine the synthesized compound's appropriateness as a potential drug candidate, the druglikeness evaluation of the compounds **15a**, **15b**, and **15c** was evaluated utilizing a variety of pharmacokinetic and structural filters. With one exception (MLOGP > 4.15), the compounds satisfy Lipinski's rule of five, suggesting a slightly higher lipophilicity that may impact permeability and solubility. Additionally, it also meets the criteria set by Ghose, Veber, and Egan filters, suggesting favorable physicochemical properties for oral bioavailability. However, the compounds with one violation (XLOGP3 > 5) are displayed in Table 2, which causes them to fail the Muegge filter; this indicates that lipophilicity may be higher than ideal for drug-likeness according to this criterion. But still, a moderate likelihood of effective oral bioavailability is indicated by the bioavailability score of 0.55. Given the compound's generally encouraging drug-like properties, the observed violations indicate that additional tuning would be necessary to improve its pharmacokinetic profile and increase solubility and absorption.

3.2.3. Binding scores of target compounds with proteins 1MWT and 6KZX.

The molecular docking scores of several compounds with two protein targets, 1MWT and 6KZX, are depicted. The compounds, labelled **14a** to **15d**, have distinct chemical structures and functional groups that vary significantly. Several amino acid residues in the binding pocket of the active site of the proteins of the bacterium *E. coli* and *S. aureus*, 1MWT and 6KZX, respectively, bind all analogues. Two proteins, 1MWT and 6KZX, were studied for their interactions with various compounds (**14a** to **15d**) and are displayed in Table 3 below. With binding scores of -6.5 kcal/mol for 1MWT and -8.2 kcal/mol for 6KZX, the compound **14e** had the highest binding affinity for both proteins among all studied substances. In comparison to the other compounds, these values indicate that compound **14e** forms the most stable contact with both proteins (1MWT and 6KZX). While the compounds **14b** and **14c** (-8.1 kcal/mol each) exhibited significant binding for 6KZX, the compounds **14c** and **14d** had the second-best binding affinity for 1MWT (-6.3 kcal/mol each). According to these binding data, the compound 14e might have the best structural features, improving its ability to interact with both proteins' binding sites.

Table 3. Binding scores of compounds.

Compound	Structure	Binding score (kcal/mol)	
		1MWT	6KZX
14a	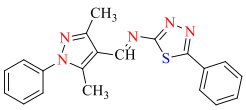	**-5.9**	**-8.0**
14b	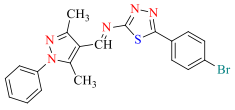	**-6.2**	**-8.1**
14c	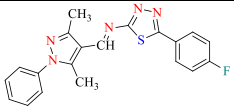	**-6.3**	**-8.1**
14d	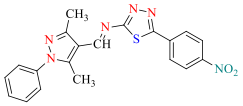	**-6.3**	**-7.8**

Compound	Structure	Binding score (kcal/mol)	
		1MWT	6KZX
14e	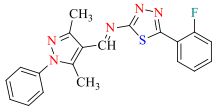	**-6.5**	**-8.2**
15a	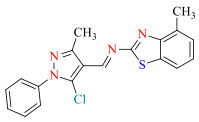	**-6.1**	**-8.0**
15b	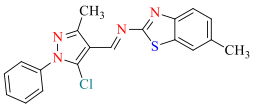	**-6.0**	**-7.9**
15c	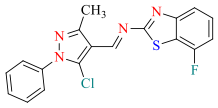	**-6.1**	**-7.9**
15d	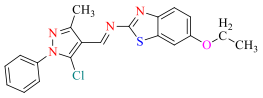	**-5.9**	**-7.8**
Ciprofloxacin	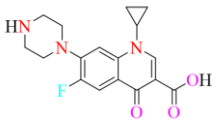	**-**	**-7.1**
Vancomycin	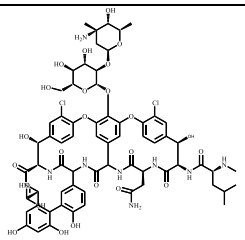	**-8.1**	**-**

3.2.4. Interaction of **14a** to **15d** with the targeted proteins.

The PDB IDs of two distinct proteins, 1MWT and 6KZX, are used to identify the interactions between different compounds and protein residues, as mentioned in Table 5. Every compound, including the compounds **14a**, **14b**, **14c**, **14d**, **14e**, **15a**, **15b**, **15c**, and **15d,** interacts in a different way with particular protein residues. The type of molecular interaction, the ligand (atom or functional group) that participates, the residue involved, and the bond distance in angstroms (Å) are the characteristics that identify the interactions. Different compounds form interactions with residues for PDB ID: 1MWT, including GLU 539, ASN 540, GLN 353, LYS 334, and VAL 160. Hydrogen bonds, halogen interactions, pi-anion, pi-cation, pi-sigma, and pi-alkyl interactions are the most often reported interaction types. In compound **14a**, for example, GLU 539 exhibits a π-anion contact with the π-ring of pyrazole at a bond distance of 3.52 Å. With a bond distance of 1.97 Å, the compound **14e** also shows a conventional hydrogen bond between LYS 334 and the nitrogen in the thiadiazole ring, demonstrating a strong hydrogen bond. A variety of interactions are observed with other compounds, such as fluorine-based halogen bonding (14c, 15c) and alkyl interactions with bromine (14b), as shown in Table 4. Molecular docking 3D interaction of protein (1MWT and 6KZX, respectively)-ligand with synthesized compounds as shown in Figure 5, respectively. Molecular docking studies were performed using the standard drugs vancomycin and Ciprofloxacin against the target proteins 1MWT and 6KZX. The obtained binding scores were –8.1 and –7.1, respectively.

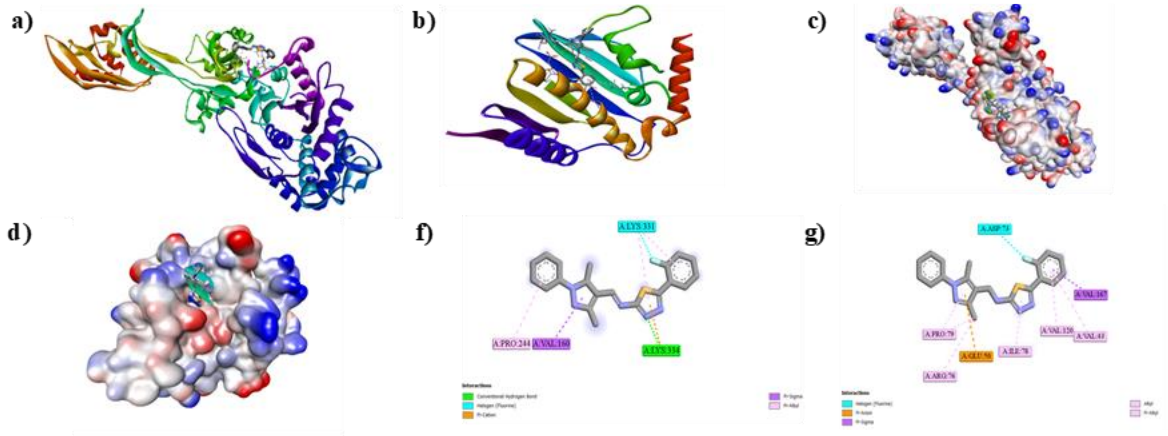

Figure 5. Molecular docking of 14e with 1MWT and 6KZX proteins **(a, b)** protein ligand complex of the compound 14e with the active site of 1MWT and 6KZX, respectively; **(c, d)** Interaction inside the binding pocket of 1MWT and 6KZX; **(e, f)** 2D interaction of 14e with 1MWT and 6KZX.

Table 4. Profiling the binding characteristics of target compounds with the proteins.

Protein PDB ID	Compound	Residue involved	Ligand	Interaction type	Bond dis.(Å)
1MWT	14a	**GLU:539**	**Carbon**	**Hydrogen bond**	**3.38**
		GLU:539	π-ring of pyrazole	Pi-Anion	3.52
		ASN:540	Nitrogen in Thiadiazole	Hydrogen Bond	3.57
		GLN:353	π-ring of benzene	Pi-Sigma	3.96
	14b	GLU:539	π-ring of benzene	Pi-Anion	3.93
		GLU:539	π-ring of thiadiazole	Pi-anion	4.05
		ILE:568	Bromine	Alkyl	4.15
		LYS:565	Bromine	Alkyl	4.23
	14c	LYS:334	π-ring of thiadiazole	Pi-cation	2.34
		GLU:655	Fluorine	Halogen	3.08
		VAL:160	π-ring of pyrazole	Pi-sigma	3.51
		LYS:331	π-ring of benzene	Pi-alkyl	3.84
	14d	GLU:539	π-ring of benzene	Pi-anion	3.39
	14e	LYS:334	Nitrogen in the thiadiazole ring	Hydrogen bond	1.97
		LYS:334	π-ring of thiadiazole	Pi-cation	2.61
		LYS:331	Fluorine	Halogen	3.24
		VAL:160	π-ring of pyrazole	Pi-sigma	3.49
		LYS:331	π-ring of benzene	Pi-alkyl	3.69
	15a	GLU:539	Carbon	Hydrogen bond	3.49
		PRO:625	π-aromatic	Pi-alkyl	4.15
		ILE:568	Methyl group	Alkyl	4.23
		GLU:539	π-aromatic	Pi-anion	4.45
		LYS:565	π-aromatic	Pi-alkyl	4.99
	15b	LYS:334	Nitrogen	Hydrogen bond	2.23
		VAL:160	π-aromatic	Pi-sigma	3.46
		LYS:331	π-aromatic	Pi-alkyl	3.84
		LYS:331	Methyl group	Alkyl	4.36
		LYS:331	π-aromatic	Pi-alkyl	4.66
	15c	GLU:539	Carbon	Hydrogen bond	3.22
		ASN:569	Fluorine	Halogen	3.26
		PRO:625	π-aromatic	Pi-alkyl	4.15
		GLU:539	π-ring of thiadiazole	Pi-anion	4.27
		LYS:565	π-aromatic	Pi-alkyl	4.81
		ILE:568	π-aromatic	Pi-alkyl	4.81
	15d	GLU:539	π-aromatic	Pi-anion	3.35
		GLU:539	π-ring of thiazole	Pi-anion	3.73
	Vancomycin	ASP:623	NH group	Hydrogen bond	1.79
		GLU:539	Oxygen-hydrogen bond	Hydrogen bond	2.28
		GLU:539	Oxygen-hydrogen bond	Hydrogen bond	2.46
		LYS:622	Hydrogen bond donor	Hydrogen bond	2.91
		ASN:541	Oxygen-hydrogen bond	Hydrogen bond	2.94
		ASP:665	Oxygen atoms in the ligand ring	Attractive charge	4.16
		ASP:665	Oxygen atoms in the ligand ring	Attractive charge	4.59

Protein PDB ID	Compound	Residue involved	Ligand	Interaction type	Bond dis.(Å)
		ASP:665	Oxygen atoms in the ligand ring	Attractive charge	4.92
		LYS:663	Alkyl interaction	Alkyl	5.09
6KZX	14a	ARG:76	Nitrogen	Hydrogen bond	2.29
		GLU:50	Carbon	Hydrogen bond	2.90
		THR:165	Nitrogen	Hydrogen bond	3.13
		ARG:76	π-ring of thiazole	Pi-Anion	3.37
		GLU:50	π-ring of thiazole	Pi-Anion	3.65
		ALA:53	π-ring of benzene	Pi-Sigma	3.78
		ASP:73	π-aromatic	Pi-cation	4.35
		ILE:78	π-aromatic	Pi-alkyl	4.62
		ILE:78	Methyl group	Alkyl	4.95
		VAL:120	π-ring of benzene	Pi-alkyl	5.01
	14b	ARG:76	Nitrogen in thiadiazole	Hydrogen bond	2.30
		GLU:50	Carbon	Hydrogen bond	2.93
		ARG:76	π-ring of thiadiazole	Pi-cation	3.42
		GLU:50	π-ring of thiadiazole	Pi-cation	3.65
		ALA:53	π-ring of benzene	Pi-sigma	3.70
		ASP:73	π-ring of pyrazole	Pi-cation	4.40
		ILE:78	π-ring of pyrazole	Pi-alkyl	4.58
		ILE:78	Methyl group	Alkyl	4.89
		VAL:120	π-ring of benzene	Pi-alkyl	4.94
	14c	GLU:50	Nitrogen	Hydrogen bond	3.31
		ARG:76	π-aromatic	Pi-cation	3.72
		ILE:78	π-ring of Thiadiazole	Pi-alkyl	4.33
		PRO:79	π-aromatic	Pi-alkyl	4.39
		GLU:50	π-aromatic	Pi-anion	4.48
		VAL:167	π-aromatic	Pi-alkyl	4.89
		VAL:120	π-aromatic	Pi-alkyl	4.90
	14d	ARG:76	Nitrogen	Hydrogen bond	2.29
		GLU:50	Carbon	Carbon hydrogen bond	2.94
		ARG:76	π-aromatic	Pi-anion	3.41
		GLU:50	π-aromatic	Pi-cation	3.65
		ALA:53	π-aromatic	Pi-sigma	3.70
		ASP:73	π-aromatic	Pi-anion	4.42
		ILE:78	π-aromatic	Pi-alkyl	4.58
		ILE:78	Methyl group	Alkyl	4.90
		VAL:120	π-aromatic	Pi-alkyl	4.92
	14e	ASP:73	Fluorine	Halogen	2.96
		VAL:167	π-aromatic	Pi-sigma	3.99
		ARG:76	Methyl group	Alkyl	4.03
		ILE:78	π-aromatic	Pi-alkyl	4.35
		PRO:79	π-aromatic	Pi-alkyl	4.42
		GLU:50	π-aromatic	Pi-anion	4.47
		PRO:79	Methyl group	Alkyl	4.81
		VAL:120	π-aromatic	Pi-alkyl	4.90
	15a	GLU:50	Carbon	Carbon hydrogen bond	3.15
		ASP:73	Nitrogen	Hydrogen bond	3.38
		ARG:76	π-aromatic	Pi-anion	3.65
		ARG:76	π-aromatic	Pi-cation	3.66
		ALA:53	Methyl group	Alkyl	3.85
		ILE:78	π-aromatic	Pi-alkyl	4.59
		ILE:78	Methyl group	Alkyl	4.99
		GLU:50	Carbon	Carbon hydrogen bond	3.15
	15b	GLU:50	Carbon atom	Carbon hydrogen bond	3.23
		ASP:73	Nitrogen	Hydrogen bond	3.36
		ARG:76	π-aromatic	Pi-anion	3.68
		ARG:76	π-aromatic	Pi-cation	3.69
		GLU:50	π-aromatic	Pi-cation	4.13
		ILE:78	π-aromatic	PI-alkyl	4.56
		ILE:78	Methyl group	Alkyl	4.99
	15c	THR:165	Nitrogen	Hydrogen bond	2.97
		GLU:50	Carbon	Hydrogen bond	3.21
		ASP:73	Nitrogen	Hydrogen bond	3.34
		ARG:76	π-aromatic	Pi-anion	3.67
		ARG:76	π-aromatic	Pi-cation	3.68

Protein PDB ID	Compound	Residue involved	Ligand	Interaction type	Bond dis.(Å)
		GLU:50	π-aromatic	Pi-cation	4.16
		ILE:78	π-aromatic	Pi-alkyl	4.57
		ILE:78	Methyl group	Alkyl	5.01
	15d	ALA:47	Methyl group	Alkyl	3.74
		VAL:71	Methyl group	Alkyl	4.17
		ARG:76	Methyl group	Alkyl	4.17
		GLU:50	π-aromatic	Pi-anion	4.42
		PRO:79	π-aromatic	Pi-alkyl	4.45
		ILE:78	π-ring of thiadiazole	Pi-alkyl	4.68
		PRO:79	Methyl group	Alkyl	4.98
	Ciprofloxacin	GLY:77	Carbonyl oxygen (C=O)	Hydrogen bond	2.31
		THR:165	Carbonyl oxygen (C=O)	Hydrogen bond	2.44
		PRO:79	Carbonyl oxygen (C=O)	Carbon-hydrogen bond	3.62
		ILE:78	Aromatic π-ring	Pi-alkyl interaction	4.41
		ILE:94	Aromatic π-ring	Pi-alkyl interaction	4.59
		ILE:94	Aromatic π-ring	Alkyl interaction	4.89

For PDB ID: 6KZX, interactions occur with residues such as ALA 53, ARG 76, GLU 50, ASP 73, and ILE 78. Pi-sigma, pi-anion, pi-cation, conventional hydrogen bonding, and alkyl interactions are the most common kinds of interactions. For example, the compound **14a** interacts with the π-ring of benzene at ALA 53 (3.78 Å) through a pi-sigma interaction and with ARG 76 (2.29 Å) via a conventional hydrogen bond. The compound **15a** interacts with THR 165 by a conventional hydrogen bond (2.98 Å) and interacts with other residues in a number of pi-alkyl and pi-anion interactions. Remarkably, the compound **15d** has a number of methyl-group alkyl interactions, including those with ALA 47, VAL 71, and ARG 76. These interactions typically promote hydrophobic interactions that stabilize the ligand-protein binding.

3.3. Antibacterial activity.

The antibacterial activity of all synthesized pyrazole derivatives was tested against gram-negative and gram-positive bacteria, as shown in Table 5, with zone of inhibition (in mm) measured using Ampicillin (5 µg/mL) and Ciprofloxacin (10 µg/mL) as standard drugs.

Table 5. Antibacterial profiling of compounds **14(a-e)** and **15(a-d)** against pathogenic *E. coli* and *S. aureus* based on three biological replicates (n = 3).

The zone of inhibition measured in mm

Compounds	Concentration in µg/mL									
	E. coli					*S. aureus*				
	50	**40**	**30**	**20**	**10**	**50**	**40**	**30**	**20**	**10**
14a	13±0.22	11±0.20	10±0.18	08±0.08	R	13±0.21	11±0.13	10±0.12	08±0.31	07±0.33
14b	14±0.09	12±0.20	10±0.15	08±0.21	07±0.19	15±0.33	13±0.13	10±0.16	08±0.15	07±0.20
14c	17±0.10	15±0.15	12±0.19	09±0.13	08±0.15	19±0.16	17±0.10	14±0.21	09±0.12	07±0.16
14d	15±0.33	11±0.21	10±0.16	09±0.10	07±0.17	16±0.28	14±0.15	11±0.18	10±0.21	7±0.21
14e	19±0.18	16±0.13	13±0.33	10±0.14	09±0.14	22±0.10	18±0.23	15±0.12	11±0.16	09±0.12
15a	15±0.27	13±0.34	10±0.23	09±0.11	08±0.13	14±0.09	12±0.21	09±0.19	08±0.12	07±0.28
15b	12±0.25	10±0.19	09±0.11	07±0.10	R	11±0.25	09±0.32	07±0.14	R	R
15c	14±0.22	11±0.20	10±0.18	08±0.08	R	13±0.27	11±0.34	10±0.11	08±0.14	07±0.10
15d	11±0.26	10±0.17	09±0.14	R	R	10±0.18	08±0.17	07±0.8	R	R
Ampicillin (5 µg/mL)			**19**			**Ampicillin (5 µg/mL)**			**23**	
Ciprofloxacin (10 µg/mL)			**25**			**Ciprofloxacin (10 µg/mL)**			**21**	

Values are means of triplicate ± standard error, R: resistant.

Compounds **14c** and **14e** showed significant activity against E. coli, with inhibition zones of 17±0.10 and 19±0.18 mm, and against S. aureus, with inhibition zones of 19±0.16 and 22±0.10 mm, at the highest concentration of 50 µg/mL, respectively. Compounds **14a**, **14b**, **14d**, **15a**, and **15c** showed moderate inhibition at 50 µg/mL concentration against both bacteria.

Compounds **14c** and **14e** also showed moderate activity with inhibition zone 15±0.15 mm, 16±0.13 mm for *E. coli* and 17±0.10 mm, 18±0.23 mm against *S. aureus* at mild concentrations at 40 µg/mL. The compound **15b** was found to be inactive at 10 µg/mL against both microorganisms, while the compound **15c** was inactive at 10 µg/mL against only *E. coli*, and the compound **15d** was inactive at 20 µg/mL and 10 µg/mL for both organisms, respectively. The trend of activity was observed as follows: R = 2F (**14e**) > 4F (**14c**) > 4Me (**15a**) > 4NO_2 (**14d**) > 4Br (**14b**) > 7F (**15c**) > H (**14a**). It is obvious that the presence of a pharmacophore, such as a fluoro substituent with lipophilic and permeability properties, increases the antimicrobial activity.

3.4. Antioxidant activity.

3.4.1. DPPH activity.

The synthesized compounds were evaluated as antioxidants by the DPPH assay at different concentrations. Vitamin C was used as a drug reference. The antioxidant activity was tested using "1,1-diphenyl-2-picrylhydrazyl radical (DPPH$^{\bullet}$)" as a stable radical compound. Its oxidation process is widely used to assess the free radical scavenging or hydrogen-donating capacity after an *in vitro* test. Based on the provided DPPH data, a clear structure-activity relationship is evident, with the unsubstituted phenyl derivative (**14a**) exhibiting the highest percentage of radical scavenging (70.29%). The introduction of substituents on the phenyl ring generally reduces antioxidant activity, with the ortho-fluoro group (**14e**, 65.67%) being less detrimental than the para-fluoro (**14c**, 55.96%) and notably less than the para-bromo (**14b**, 49.13%) and para-nitro (**14d**, 52.60%) groups. This suggests that the strong electron-withdrawing nature of the nitro and bromo groups, particularly in the para position, significantly decreases the molecule's ability to donate electrons and scavenge free radicals. The benzothiazole-based derivatives exhibited a broader range of activity, generally lower than the phenyl compounds, with the 6-ethoxy derivative (**15d**, 55.96%) showing the highest activity among its pyrazole-benzothiazole analogs. Its activity was comparable to the para-fluoro phenyl derivative, suggesting that the ethoxy group enhances scavenging potential within the benzothiazole scaffold. Conversely, the methyl groups in the 4-position (**15a**, 45.58%) and 6-position (**15b**, 43.17%), and the 7-fluoro group (**15c**, 48.75%), yielded lower activity, demonstrating that the nature and position of the substituent are critical determinants of the final antioxidant efficacy, as shown in Table 6. The compound **14e** showed significant activity across all concentrations compared to the other synthesized compounds. The DPPH activity of the tested compounds can be ordered as follows: **Vitamin C** > **14e** > **14a** > **14c-15d** > **14d** > **14b** > **15c** > **15a** > **15b**, as shown in Figure 6.

Table 6. *In vitro* evaluation of the radical scavenging activity of **14(a-e)** and **15(a-d)**

Compounds	Percentage of inhibition (%I)					
	Blank	20 µg/mL	40 µg/mL	60 µg/mL	80 µg/mL	100 µg/mL
14a	0.00	14.33	29.42	52.21	59.23	70.29
14b	0.00	4.52	16.35	21.15	32.60	49.13
14c	0.00	7.50	28.08	35.67	46.73	55.96
14d	0.00	10.00	17.88	27.79	40.19	52.60
14e	0.00	11.35	16.92	33.08	50.10	65.67
15a	0.00	1.73	10.58	21.83	35.48	45.58
15b	0.00	2.21	10.29	20.58	32.12	43.17
15c	0.00	3.08	12.12	25.58	37.88	48.75
15d	0.00	8.27	29.33	36.25	48.17	55.96
Vitamin-C	0.00	5.29	45.98	79.20	84.94	86.90

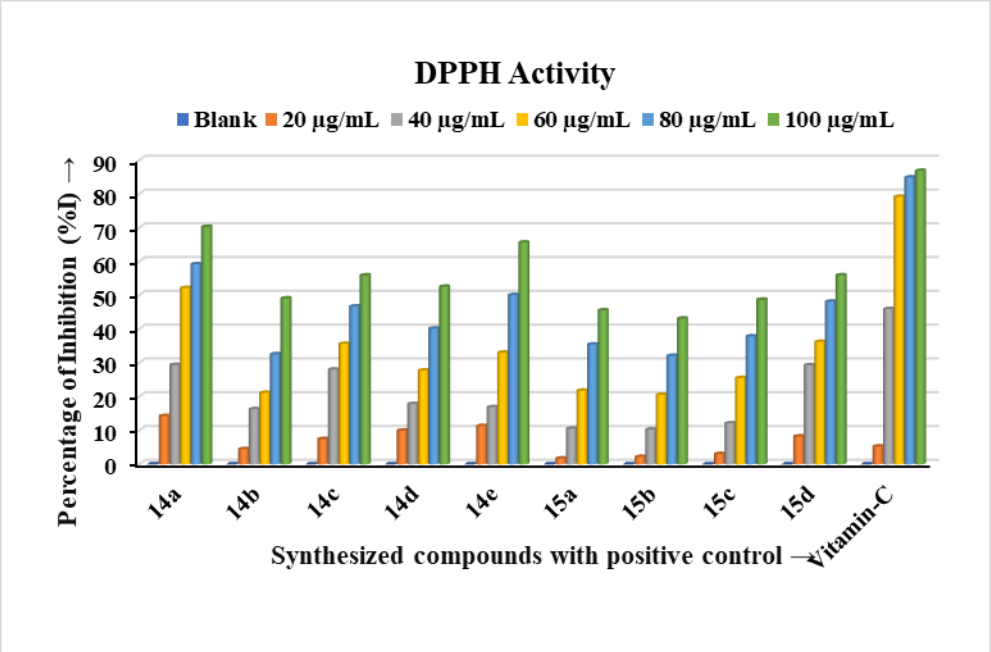

Figure 6. Comparison of DPPH Activity of synthesized compounds with reference drug.

3.4.2. FRAP activity.

All synthesized compounds showed more potent FRAP activity than the standard, ascorbic acid, at all concentrations, as shown in Table 7. Based on the FRAP data, which shows that a higher net OD corresponds to greater antioxidant activity, clear substituent effects are observed across the derivatives. For the substituted phenyl compounds, the position and electronic nature of the group significantly alter the activity, with the ortho-fluoro derivative (**14e**) displaying the highest activity (OD 0.46), surpassing both the para-fluoro (**14c**, OD 0.37) and the unsubstituted (**14a**, OD 0.33) phenyl derivatives. This indicates that the ortho position is particularly favorable for enhancing FRAP activity, possibly due to intramolecular effects. Conversely, the strong electron-withdrawing para-nitro group (**14d**) resulted in the lowest activity among the phenyl derivatives (OD 0.31), showing the effect of electron-withdrawing character. When comparing the benzothiazole derivatives, the 7-fluoro-substituted compound (**15c**, OD 0.29) exhibited a slightly higher antioxidant capacity than the 6-ethoxy derivative (**15d**, OD 0.25). However, both were less active than the pyrazole-thiadiazole derivatives, with **15d** being the least active overall, as shown in Figure 7. These results collectively demonstrate that both the electronic properties and the precise location of the substituents are critical determinants of the antioxidant potency in these molecular scaffolds.

Table 7. A comparative ferric-reducing antioxidant potential of target compounds with vitamin C.

Compounds	Net OD at 593 nm					
	Blank	20 µg/mL	40 µg/mL	60 µg/mL	80 µg/mL	100 µg/mL
14a	0	0.96	0.69	0.57	0.51	0.33
14c	0	1.07	0.74	0.61	0.52	0.37
14d	0	0.88	0.66	0.55	0.48	0.31
14e	0	1.17	0.77	0.64	0.55	0.46
15c	0	0.81	0.62	0.52	0.43	0.29
15d	0	0.73	0.55	0.43	0.36	0.25
Vitamin-C	0	0.67	0.52	0.39	0.27	0.15

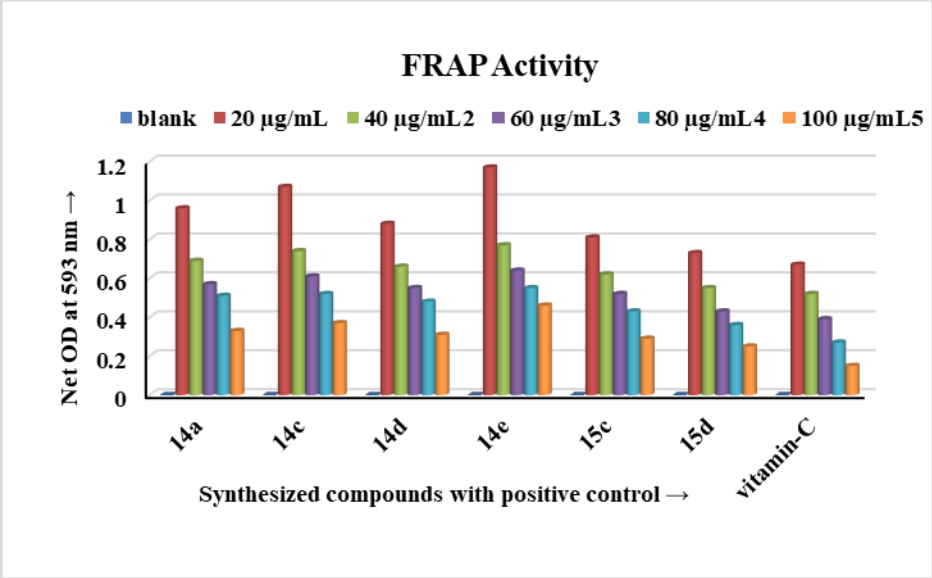

Figure 7. Comparison of the FRAP activity of novel compounds and a reference.

3.5. Anticancer activity.

The cytotoxic activity of newly synthesized heterocycles (**14a**, **14c**, **14d**, **14e**, **15c**, and **15d**) was evaluated against two breast cancer cell lines, MDA-MB-231 and MCF-7. The results obtained are summarized in Table 8. Among the tested derivatives, the compound **14e** exhibited the highest cytotoxicity, with a percentage inhibition of 68.49 and 57.38 at 1000 µg/mL against both MCF-7 and MDA-MB-231, respectively. In comparison, the compound **14c** displayed slightly lower cytotoxic activity than the compound **14e** against both cell lines. Furthermore, the compounds **14e** and **14c** showed marked sensitivity to MDA-MB-231 cells with %PI 50.04 and 41.01 at 1 µM, respectively, as shown in Figure 8. Conversely, compounds **14e** and **14c** exhibited higher sensitivity to MCF-7 cells, indicating that structural variations in pyrazole derivatives influence their selectivity between these two breast cancer cell lines. Overall, the derivatives containing fluoro at the 2nd and 4th positions (14e and 14c) demonstrated the highest sensitivity at 1000 µM against both tested cell lines, warranting further investigation of their antitumor potential among the tested pyrazole derivatives. These studies have established that the anticancer properties of pyrazole Schiff bases are closely linked to the presence of electron-withdrawing groups. Consistently, in this study, compounds containing electron-withdrawing substituents, such as 14e and 14c, exhibited superior cytotoxicity against breast cancer cell lines, reinforcing their potential as promising anticancer agents.

Table 8. Assessing the cytotoxic potential of compound series **14(a, c, d**, and **e)** and **15 (c** and **d)** via percentage inhibition.

Compounds	% Inhibition									
	Vehicle control*	Positive control**	At different concentrations against MDA-MB-231			Vehicle control*	Positive control**	At different concentrations against MCF-7		
			1 µM	500 µM	1000 µM			1 µM	500 µM	1000 µM
14a	0.79	75.30	3.80	16.62	30.40	3.63	61.04	3.4	13.54	19.55
14c	0.79	75.30	41.01	49.88	59.22	3.63	61.04	39.03	48.29	51.22
14d	0.79	75.30	3.72	18.69	28.74	3.63	61.04	2.75	12.56	17.91
14e	0.79	75.30	50.04	53.84	68.49	3.63	61.04	41.17	53.03	57.38
15c	0.79	75.30	7.68	23.04	36.03	3.63	61.04	34.44	40.42	48.78
15d	0.79	75.30	2.85	14.17	27.63	3.63	61.04	7.16	10.44	14.63

DMSO** ****Cisplatin

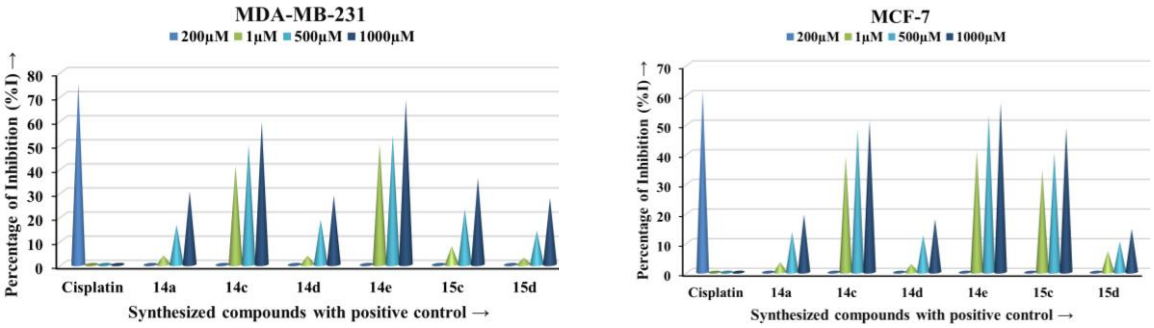

Figure 8. Comparison of cytotoxicity assessment of the target compounds.

3.6. Structure–activity relationship (SAR) of pyrazole–thiadiazole derivatives.

The structure-activity relationship (SAR) of newly synthesized compounds **14(a-e)** and **15(a-d)** has been depicted in Figure 9. In the antioxidant assays (DPPH and FRAP), the unsubstituted phenyl derivative consistently shows the highest activity, suggesting that the core structure is inherently potent for scavenging radicals and that most substituents reduce this effect. Electron-withdrawing groups (EWGs) generally decrease antioxidant activity, as seen with the para-bromo and para-nitro groups, which destabilize the radical intermediate. However, the substituent position is also crucial, as the ortho-fluoro group shows significantly higher activity than its para-fluoro counterpart, suggesting a potential intramolecular effect that enhances its scavenging capacity.

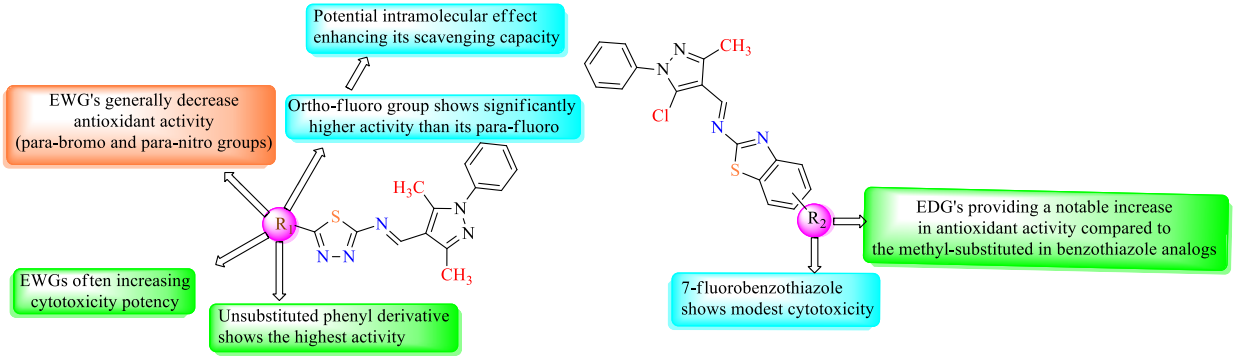

Figure 9. SAR of substituted pyrazole-thiadiazole derivatives.

The benzothiazole derivatives generally exhibit lower antioxidant activity, with the electron-donating ethoxy group providing a notable increase in activity compared to the methyl-substituted and fluoro-substituted derivatives, highlighting the positive influence of EDGs in this scaffold. For cytotoxicity against MDA-MB-231 and MCF-7 cell lines, the SAR shifts, with EWGs often increasing potency. The ortho-fluoro derivative shows the highest inhibition for both MDA-MB-231 and MCF-7 cells, surpassing the unsubstituted derivative. The para-fluoro derivative also shows enhanced cytotoxicity compared to the unsubstituted one. The lower cytotoxicity of the para-nitro and para-bromo derivatives compared to the fluoro-substituted ones suggests that an optimal balance of electronic and steric factors, rather than just the presence of EWGs, is critical for modulating anticancer activity in these cell lines. Furthermore, the 7-fluorobenzothiazole shows modest activity, suggesting that cytotoxicity is highly dependent on the specific molecular framework and substituent combination. This comparative analysis across assays reveals that the electronic and positional effects of substituents yield distinct SARs for distinct biological activities, underscoring the need for targeted design to optimize specific pharmacological profiles.

4. Conclusions

A novel series of pyrazole-containing 1,3,4-thiadiazole (**14a-e**) and benzothiazole (**15a-d**) Schiff base heterocycles was successfully synthesized and characterized. The structural novelty lies in the fusion of the pyrazole core with both thiadiazole and benzothiazole moieties *via* a Schiff base linkage; synthetic strategies were confirmed by spectroscopic analysis. Molecular docking studies validated the high potential of compound **14e**, revealing its strong binding affinity and favorable interactions with key target proteins, positioning it as a promising multi-target inhibitor. The *in silico* ADMET analysis confirmed the drug-likeness of the most active compounds, including **14e**, indicating their potential for oral bioavailability and overall therapeutic efficacy. This multi-pronged investigation, integrating innovative synthetic chemistry with rigorous pharmacological and computational analysis, provides a strong basis for further optimization. The findings underscore the translational potential of these pyrazole derivatives as promising lead compounds for developing new therapeutic agents, particularly in the fight against breast cancer and microbial infections, by leveraging their distinct SAR profiles.

The compound **14e**, containing a specific ortho-fluoro substituent, emerged as a multifaceted lead, exhibiting potent antibacterial activity against *E. coli* and *S. aureus*, significant antioxidant activity, and the highest cytotoxicity against both breast cancer cell lines. Comprehensive pharmacological evaluation revealed that the biological activity of target compounds is strongly influenced by specific substituents, as established through structure-activity relationship (SAR) studies. For antioxidant activity, the unsubstituted phenyl derivative (**14a**) demonstrated the highest potency in the DPPH assay, suggesting that the pyrazole–thiadiazole scaffold is inherently a potent radical scavenger. In contrast, for cytotoxicity against triple-negative (MDA-MB-231) and estrogen receptor-positive (MCF-7) breast cancer cell lines, electron-withdrawing groups (EWGs), particularly the ortho-fluoro group, were associated with increased potency, highlighting distinct SARs for different biological targets.

Author Contributions

Conceptualization, U.K.B. and S.N.; methodology, M.C.R.; software, V.B; validation, V.B. and M.C; formal analysis, S.N.S.; investigation, N.G.S; writing—original draft preparation, M.C.R; writing—review and editing, V.B; supervision, U.K.B. All authors have read and agreed to the published version of the manuscript.

Institutional Review Board Statement

Not applicable.

Informed Consent Statement

Not applicable.

Data Availability Statement

Data supporting the findings of this study are available upon reasonable request from the corresponding author.

Funding

This research received no external funding.

Acknowledgments

The authors greatly thank The Principal and Management, Yuvaraja's College, University of Mysore, Mysuru, Karnataka, India, and Vidyavardhaka College of Engineering, Visvesvaraya Technological University, Mysuru, Karnataka, India, for providing support and an instrumentation facility.

Conflicts of Interest

The authors declare no conflict of interest.

Abbreviations

The following abbreviations are used in this manuscript:

Abbreviation	Definition
ADMET	Absorption, Distribution, Metabolism, Excretion, Toxicity
AMR	Antimicrobial resistance
ALS	Amyotrophic Lateral Sclerosis
DPPH	2,2-Diphenyl-1-picrylhydrazyl
E. coli	*Escherichia coli*
S. aureus	*Staphylococcus aureus*
FRAP	Ferric Reducing Antioxidant Power
Fe^{2+}-TPTZ	Ferrous-2,4,6-tripyridyl-s-triazine
MCF-7	Michigan Cancer Foundation-7
MDA-MB-231	M D Anderson - Metastatic Breast - 231
SRB	Sulforhodamine B
XO	Xanthine oxidase

References

1. Biswas, T.; Mittal, R.K.; Sharma, V.; Kanupriya; Mishra, I. Nitrogen-fused Heterocycles: Empowering Anticancer Drug Discovery. *Med. Chem.* **2024**, *20*, 369-384, https://doi.org/10.2174/0115734064278334231211054053.
2. Peerzade, N.A.; Jadhav, S.Y.; Bhosale, R.B.; Masand, V.H.; Gawali, R.G.; Al-Hussain, S.A.; Al-Mutairi, A.A.; Zaki, M.E.A. Pyrazole-based N-phenyl pyrazolines: Synthesis, docking, and pharmacological evaluation. *Res. Chem.* **2024**, *11*, 101793, https://doi.org/10.1016/j.rechem.2024.101793.
3. Laamari, Y.; Fawzi, M.; Hachim, M.E.; Bimoussa, A.; Oubella, A.; Ketatni, E.M.; Saadi, M.; Ammari, L.E.; Itto, M.Y.A.; Morjani, H.; Khouili, M.; Auhmani, A. Synthesis, characterization and cytotoxic activity of pyrazole derivatives based on thymol. *J. Mol. Struct.* **2024**, *1297*, 136864, https://doi.org/10.1016/j.molstruc.2023.136864.
4. Ramoba, L.V.; Nzondomyo, W.J.; Serala, K.; Macharia, L.W.; Biswas, S.; Prince, S.; Malan, F.P.; Alexander, O.T.; Manicum, A.-L.E. Derivatives of Pyrazole-Based Compounds as Prospective Cancer Agents. *ACS Omega* **2025**, *10*, 12671-12678, https://doi.org/10.1021/acsomega.5c00320.
5. Xu, Z.; Zhuang, Y.; Chen, Q. Current scenario of pyrazole hybrids with *in vivo* therapeutic potential against cancers. *Eur. J. Med. Chem.* **2023**, *257*, 115495, https://doi.org/10.1016/j.ejmech.2023.115495.
6. Naghavi, M.; Vollset, S.E.; Ikuta, K.S.; Swetschinski, L.R.; Gray, A.P.; Wool, E.E.; Robles Aguilar, G.; Mestrovic, T.; Smith, G.; Han, C.; Hsu, R.L.; Chalek, J.; Araki, D.T.; Chung, E.; Raggi, C.; Gershberg Hayoon, A.; Davis Weaver, N.; Lindstedt, P.A.; Smith, A.E.; Altay, U.; Bhattacharjee, N.V.; Giannakis, K.; Fell, F.; McManigal, B.; Ekapirat, N.; Mendes, J.A.; Runghien, T.; Srimokla, O.; Abdelkader, A.; Abd-Elsalam, S.; Aboagye, R.G.; Abolhassani, H.; Abualruz, H.; Abubakar, U.; Abukhadijah, H.J.; Aburuz, S.; Abu-Zaid, A.; Achalapong, S.; Addo, I.Y.; Adekanmbi, V.; Adeyeoluwa, T.E.; Adnani, Q.E.S.; Adzigbli, L.A.; Afzal, M.S.; Afzal, S.; Agodi, A.; Ahlstrom, A.J.; Ahmad, A.; Ahmad, S.; Ahmad, T.; Ahmadi, A.;

Ahmed, A.; Ahmed, H.; Ahmed, I.; Ahmed, M.; Ahmed, S.; Ahmed, S.A.; Akkaif, M.A.; Al Awaidy, S.; Al Thaher, Y.; Alalalmeh, S.O.; AlBataineh, M.T.; Aldhaleei, W.A.; Al-Gheethi, A.A.S.; Alhaji, N.B.; Ali, A.; Ali, L.; Ali, S.S.; Ali, W.; Allel, K.; Al-Marwani, S.; Alrawashdeh, A.; Altaf, A.; Al-Tammemi, A.B.; Al-Tawfiq, J.A.; Alzoubi, K.H.; Al-Zyoud, W.A.; Amos, B.; Amuasi, J.H.; Ancuceanu, R.; Andrews, J.R.; Anil, A.; Anuoluwa, I.A.; Anvari, S.; Anyasodor, A.E.; Apostol, G.L.C.; Arabloo, J.; Arafat, M.; Aravkin, A.Y.; Areda, D.; Aremu, A.; Artamonov, A.A.; Ashley, E.A.; Asika, M.O.; Athari, S.S.; Atout, M.M.d.W.; Awoke, T.; Azadnajafabad, S.; Azam, J.M.; Aziz, S.; *et al*. Global burden of bacterial antimicrobial resistance 1990–2021: a systematic analysis with forecasts to 2050. *Lancet* **2024**, *404*, 1199-1226, https://doi.org/10.1016/S0140-6736(24)01867-1.

7. Pancu, D.F.; Scurtu, A.; Macasoi, I.G.; Marti, D.; Mioc, M.; Soica, C.; Coricovac, D.; Horhat, D.; Poenaru, M.; Dehelean, C. Antibiotics: Conventional Therapy and Natural Compounds with Antibacterial Activity—A Pharmaco-Toxicological Screening. *Antibiotics* **2021**, *10*, 401, https://doi.org/10.3390/antibiotics10040401.
8. Reheim, M.A.M.A.; Rady, H.S.A.; Mohamed, O.A.; Hassan, A.; Hafiz, I.S.A.; Reffat, H.M.; Elsaid, F.G.; Eldesoqui, M.; Alshaya, D.S.; Badawy, A.A.; Fayad, E.; Abdelmonsef, A.H. Synthesis, Anti-Inflammatory, and Molecular Docking Studies of New Heterocyclic Derivatives Comprising Pyrazole, Pyridine, and/or Pyran Moieties. *Pharmaceuticals* **2025**, *18*, 335, https://doi.org/10.3390/ph18030335.
9. Nehra, B.; Kumar, M.; Chawla, V.; Chawla, P.A. Current progress in synthetic and medicinal chemistry of pyrazole hybrids as potent anticancer agents with SAR studies. *Futur. J. Pharm. Sci.* **2025**, *11*, 75, https://doi.org/10.1186/s43094-025-00821-7.
10. Obeid, A.O.; Al-Aghbari, S.A.; Al-Taifi, E.A.; Alhamzi, E.H.L.; Rageh, Z. Syntheses, Characterization and Biological Effect Studies of Some New Heterocyclic Compounds Containing Pyrazole and Pyridazine Rings and Their Schiff Bases. *OALibJ* **2025**, *12*, e12623, https://doi.org/10.4236/oalib.1112623.
11. de Oliveira, Lanussy P.; de Oliveira Neto, Jerônimo R.; de Oliveira, Thiago S.; Naves, Lara M.; Marques, Stefanne M.; Cruz, Alessandro C.; Fajemiroye, James O.; Pedrino, G.; Lião, Luciano M.; Menegatti, R.; da Cunha, Luiz C. Preclinical Pharmacokinetic Assessment of a Promising Vasorelaxant, Analgesic, and Anti-Inflammatory Prototype 5-[1-(4-Fluorophenyl)-1H-pyrazol-4-yl]-2H-tetrazole (LQFM020) Through Selective Bioanalytical HPLC-PDA-Based Method. *Biomed. Chromatogr.* **2025**, *39*, e70082, https://doi.org/10.1002/bmc.70082.
12. Deshmukh, H.S.; Adole, V.A.; Wagh, S.B.; Khedkar, V.M.; Jagdale, B.S. Exploring N-heterocyclic linked novel hybrid chalcone derivatives: synthesis, characterization, evaluation of antidepressant activity, toxicity assessment, molecular docking, DFT and ADME study. *RSC Adv.* **2025**, *15*, 16187-16210, https://doi.org/10.1039/D5RA01929J.
13. Abd-Elhalim, B.T.; El-Bana, G.G.; El-Sayed, A.F.; Abdel-Ghani, G.E. Antifungal activity and biocompatibility assessment with molecular docking and dynamic simulations of new pyrazole derivatives. *BMC Biotechnol.* **2025**, *25*, 15, https://doi.org/10.1186/s12896-025-00948-8.
14. Oulous, A.; Dib, I.; Harit, T.; Alzahrani, A.Y.A.; Cherfi, M.; Daoudi, N.E.; Ziyyat, A.; Malek, F. New Pyrazole-Based Tetrazole Derivatives: Synthesis, Characterization, and Their Vasorelaxant and α-Amylase Inhibition Activities. *Chem. Biol. Drug Des.* **2025**, *106*, e70157, https://doi.org/10.1111/cbdd.70157.
15. Khuzwayo, S.S.; Selepe, M.A.; Meyer, D.; Gama, N.H. The synthesis and investigation of novel 3-benzoylbenzofurans and pyrazole derivatives for anti-HIV activity. *RSC Med. Chem.* **2025**, *16*, 2142-2158, https://doi.org/10.1039/D4MD00844H.
16. Eldehna, W.M.; Alkabbani, M.A.; Elsayed, Z.M.; Ibrahim, K.M.; Majrashi, T.A.; Elagawany, M.; Salem, R.; Abdel-Aziz, H.A.; Tawfik, H.O. Identification of Novel Triazole–Pyrazole Conjugates as Potential Anticonvulsant Agents: Synthesis and Biological Evaluations. *ACS Chem. Neurosci.* **2025**, *16*, 3038-3050, https://doi.org/10.1021/acschemneuro.5c00392.
17. Atmaram, U.A.; Roopan, S.M. Biological activity of oxadiazole and thiadiazole derivatives. *Appl. Microbiol. Biotechnol.* **2022**, *106*, 3489-3505, https://doi.org/10.1007/s00253-022-11969-0.
18. Anthwal, T.; Paliwal, S.; Nain, S. Diverse Biological Activities of 1,3,4-Thiadiazole Scaffold. *Chemistry* **2022**, *4*, 1654-1671, https://doi.org/10.3390/chemistry4040107.
19. Shosha, M.I.; El-Ablack, F.Z.; Saad, E.A. New thiazole derivative as a potential anticancer and topoisomerase II inhibitor. *Sci. Rep.* **2025**, *15*, 710, https://doi.org/10.1038/s41598-024-81294-1.
20. Andrade, I.M.G.; Lima Filho, E.d.O.; Valadão, C.F.; Forezi, L.d.S.M.; de C. da Silva, F. Recent Advances in Isatin–Thiazole Hybrids: Synthesis, Structural Design, and Biological Application. *Chem Biodivers.* **2025**, *22*, e01989, https://doi.org/10.1002/cbdv.202501989.

21. Irfan, A.; Batool, F.; Zahra Naqvi, S.A.; Islam, A.; Osman, S.M.; Nocentini, A.; Alissa, S.A.; Supuran, C.T. Benzothiazole derivatives as anticancer agents. *J. Enzym. Inhib. Med. Chem.* **2020**, *35*, 265-279, https://doi.org/10.1080/14756366.2019.1698036.
22. Bhat, M.; Belagali, S.L. Structural Activity Relationship and Importance of Benzothiazole Derivatives in Medicinal Chemistry: A Comprehensive Review. *Mini-Rev. Org. Chem.* **2020**, 17, 323-350, https://doi.org/10.2174/1570193X16666190204111502.
23. Gallego-Yerga, L.; Ceña, V.; Peláez, R. Potent and Selective Benzothiazole-Based Antimitotics with Improved Water Solubility: Design, Synthesis, and Evaluation as Novel Anticancer Agents. *Pharmaceutics* **2023**, *15*, 1698, https://doi.org/10.3390/pharmaceutics15061698.
24. Al-Mutairi, A.A.; Hafez, H.N.; El-Gazzar, A.-R.B.A.; Mohamed, M.Y.A. Synthesis and Antimicrobial, Anticancer and Anti-Oxidant Activities of Novel 2,3-Dihydropyrido[2,3-d]pyrimidine-4-one and Pyrrolo[2,1-b][1,3]benzothiazole Derivatives via Microwave-Assisted Synthesis. *Molecules* **2022**, *27*, 1246, https://doi.org/10.3390/molecules27041246.
25. Morsy, M.A.; Ali, E.M.; Kandeel, M.; Venugopala, K.N.; Nair, A.B.; Greish, K.; El-Daly, M. Screening and Molecular Docking of Novel Benzothiazole Derivatives as Potential Antimicrobial Agents. *Antibiotics* **2020**, *9*, 221, https://doi.org/10.3390/antibiotics9050221.
26. Corcia, P.; Guy, N.; Pradat, P.-F.; Soriani, M.-H.; Verschueren, A.; Couratier, P. Treatment continuity of amyotrophic lateral sclerosis with available riluzole formulations: state of the art and current challenges in a 'real-world' setting. *Amyotroph. Lateral Scler. Front. Degener.* **2025**, *26*, 15-21, https://doi.org/10.1080/21678421.2024.2375330.
27. Li, T.; Zou, S.; Zhang, Z.; Liu, M.; Liang, Z. Efficacy of pramipexole on quality of life in patients with Parkinson's disease: a systematic review and meta-analysis. *BMC Neurol.* **2022**, *22*, 320, https://doi.org/10.1186/s12883-022-02830-y.
28. Bao, Y.-W.; Shea, Y.-F.; Chiu, P.K.-C.; Kwan, J.S.K.; Chan, F.H.-W.; Mak, H.K.-F. Incremental diagnostic value of 18F-Fluetemetamol PET in differential diagnoses of Alzheimer's Disease-related neurodegenerative diseases from an unselected memory clinic cohort. *Sci. Rep.* **2022**, *12*, 10385, https://doi.org/10.1038/s41598-022-14532-z.
29. Mushtaq, I.; Ahmad, M.; Saleem, M.; Ahmed, A. Pharmaceutical significance of Schiff bases: an overview. *Futur. J. Pharm. Sci.* **2024**, *10*, 16, https://doi.org/10.1186/s43094-024-00594-5.
30. Tsacheva, I.; Todorova, Z.; Momekova, D.; Momekov, G.; Koseva, N. Pharmacological Activities of Schiff Bases and Their Derivatives with Low and High Molecular Phosphonates. *Pharmaceuticals* **2023**, *16*, 938, https://doi.org/10.3390/ph16070938.
31. Piotr, P.; Adam, H.; Krystian, P.; Bogumil, B.; Franz, B. Biological Properties of Schiff Bases and Azo Derivatives of Phenols. *Curr. Org. Chem.* **2009**, *13*, 124-148, https://doi.org/10.2174/138527209787193774.
32. Aroua, L.M.; Alkhaibari, I.S.; Alminderej, F.M.; Messaoudi, S.; Chigurupati, S.; Al-mahmoud, S.A.; Albadri, A.E.A.E.; Emwas, A.-H.; Mohammed, H.A. Synthesis, bioactivity, and molecular docking of pyrazole bearing Schiff-bases as prospective dual alpha-amylase and alpha-glucosidase inhibitors with antioxidant activity. *J. Mol. Struct.* **2025**, *1320*, 139291, https://doi.org/10.1016/j.molstruc.2024.139291.
33. Mezgebe, K.; Mulugeta, E. Synthesis and pharmacological activities of Schiff bases with some transition metal complexes: a review. *Med. Chem. Res.* **2024**, *33*, 439-463, https://doi.org/10.1007/s00044-024-03192-5.
34. Yeşil, T.A. New Azo-Azomethine Compounds: Comprehensive Evaluation of In Silico Biological Activities, ADMEt Profiling, and In Vitro Antioxidant Properties. *ChemistrySelect* **2025**, *10*, e202405875, https://doi.org/10.1002/slct.202405875.
35. Kurban, B.; Sağlık, B.N.; Osmaniye, D.; Levent, S.; Özkay, Y.; Kaplancıklı, Z.A. Synthesis and Anticancer Activities of Pyrazole–Thiadiazole-Based EGFR Inhibitors. *ACS Omega* **2023**, *8*, 31500-31509, https://doi.org/10.1021/acsomega.3c04635.
36. Ding, X.; Zhai, Z.; Lv, L.; Sun, Z.; Liu, X. Design, synthesis, biological activity and density function theory study of pyrazole derivatives containing 1,3,4-thiadiazole moiety. *Front. Chem. Sci. Eng.* **2017**, *11*, 379-386, https://doi.org/10.1007/s11705-017-1634-2.
37. Dai, H.; Ge, S.; Li, G.; Chen, J.; Shi, Y.; Ye, L.; Ling, Y. Synthesis and bioactivities of novel pyrazole oxime derivatives containing a 1,2,3-thiadiazole moiety. *Bioorg. Med. Chem. Lett.* **2016**, *26*, 4504-4507, https://doi.org/10.1016/j.bmcl.2016.07.068.

38. Abdelgawad, M.A.; Bakr, R.B.; Omar, H.A. Design, synthesis and biological evaluation of some novel benzothiazole/benzoxazole and/or benzimidazole derivatives incorporating a pyrazole scaffold as antiproliferative agents. *Bioorg. Chem.* **2017**, 74, 82-90, https://doi.org/10.1016/j.bioorg.2017.07.007.
39. Bhat, M.; Belagali, S.L. Synthesis, Characterization and Biological Screening of Pyrazole-Conjugated Benzothiazole Analogs. *Future Med. Chem.* **2018**, *10*, 71-87, https://doi.org/10.4155/fmc-2017-0138.
40. Bondock, S.; Fadaly, W.; Metwally, M.A. Synthesis and antimicrobial activity of some new thiazole, thiophene and pyrazole derivatives containing benzothiazole moiety. *Eur. J. Med. Chem.* **2010**, *45*, 3692-3701, https://doi.org/10.1016/j.ejmech.2010.05.018.
41. Schrecker, L.; Dickhaut, J.; Holtze, C.; Staehle, P.; Vranceanu, M.; Hellgardt, K.; Hii, K.K. Discovery of unexpectedly complex reaction pathways for the Knorr pyrazole synthesis *via* transient flow. *React. Chem. Eng.* **2023**, *8*, 41-46, https://doi.org/10.1039/d2re00271j.
42. Touitou, M.; Manetti, F.; Ribeiro, C.M.; Pavan, F.R.; Scalacci, N.; Zrebna, K.; Begum, N.; Semenya, D.; Gupta, A.; Bhakta, S.; McHugh, T.D.; Senderowitz, H.; Kyriazi, M.; Castagnolo, D. Improving the Potency of *N*-Aryl-2,5-dimethylpyrroles against Multidrug-Resistant and Intracellular Mycobacteria. *ACS Med. Chem. Lett.* **2020**, *11*, 638-644, https://doi.org/10.1021/acsmedchemlett.9b00515.
43. Prajuli, R.; Banerjee, J.; Khanal, H. Synthesis of Some Pyrazolone Derivatives and Evaluation of its Antibacterial and Cytotoxic Activity. *Orient. J. Chem.* **2015**, *31*, 2099-2106, https://doi.org/10.13005/ojc/310430.
44. Popov, A.V.; Kobelevskaya, V.A.; Larina, L.I.; Rozentsveig, I.B. Synthesis of poly-functionalized pyrazoles under Vilsmeier-Haack reaction conditions. *Arkivoc* **2019**, *6*, 1-14, https://doi.org/10.24820/ark.5550190.p010.934.
45. Keerthi Kumar, C.T.; Keshavayya, J.; Rajesh, T.N.; Peethambar, S.K.; Shoukat Ali, A.R. Synthesis, Characterization, and Biological Activity of 5-Phenyl-1,3,4-thiadiazole-2-amine Incorporated Azo Dye Derivatives. *Org. Chem. Int.* **2013**, *2013*, 370626, https://doi.org/10.1155/2013/370626.
46. Moradi Rufchahi, E.O.; Yousefi, H.; Mohammadinia, M. Synthesis and spectral properties of some azo disperse dyes containing a benzothiazole moiety. *J. Mol. Liq.* **2013**, *188*, 173-177, https://doi.org/10.1016/j.molliq.2013.08.021.
47. Nanjundaswamy, S.; Jayashankar, J.; Renganathan, R.R.A.; Karthik, C.S.; Mallesha, L.; Mallu, P.; Rai, V.R. Pyridine coupled pyrazole analogues as lethal weapon against MRSA: An *in-vitro* and *in-silico* approach. *Microb. Pathog.* **2022**, *166*, 105508, https://doi.org/10.1016/j.micpath.2022.105508.
48. Nanjundaswamy, S.; Jayashankar, J.; Chethana, M.H.; Renganathan, R.R.A.; Karthik, C.S.; Ananda, A.P.; Nagashree, S.; Mallu, P.; Rai, V.R. Design, synthesis, and *in-silico* studies of pyrazolylpyridine analogues: A futuristic antibacterial contender against coagulase positive superbug-MRSA. *J. Mol. Struct.* **2022**, *1255*, 132400, https://doi.org/10.1016/j.molstruc.2022.132400.
49. Shinde, S.A.; Mhetar, M.J.; Parit, A.G.; Thombre, A.R. In-silico investigation and ADMET prediction of potential antifungal phytochemicals against lanosterol 14-alpha demethylase inhibitors. *Asian J. Pharm. Res* **2024**, *14*, 33-38, https://doi.org/10.52711/2231-5691.2024.00005.
50. Bauer, A.W.; Kirby, W.M.; Sherris, J.C.; Turck, M. Antibiotic susceptibility testing by a standardized single disk method. *Am. J. Clin. Pathol.* **1966**, *45*, 493-496.
51. Surendra Kumar, R.; Arif, I.A.; Ahamed, A.; Idhayadhulla, A. Anti-inflammatory and antimicrobial activities of novel pyrazole analogues. *Saudi J. Biol. Sci.* **2016**, *23*, 614-620, https://doi.org/10.1016/j.sjbs.2015.07.005.
52. Kumara, P.; Sunil, K.; Arun Kumar, B. Determination of DPPH Free Radical Scavenging Activity by RP-HPLC, Rapid Sensitive Method for the Screening of Berry Fruit Juice Freeze Dried Extract. *Nat. Prod. Chem. Res* **2018**, *6*, 1000341, https://doi.org/10.4172/2329-6836.1000341.
53. Nariya, P.B.; Bhalodia, N.R.; Shukla, V.J.; Acharya, R.; Nariya, M.B. *In vitro* evaluation of antioxidant activity of *Cordia dichotoma* (Forst f.) bark. **2013**, *34*, 124-128, https://doi.org/10.4103/0974-8520.115451.
54. Benzie, I.F.F.; Strain, J.J. The Ferric Reducing Ability of Plasma (FRAP) as a Measure of "Antioxidant Power": The FRAP Assay. *Anal. Biochem.* **1996**, *239*, 70-76, https://doi.org/10.1006/abio.1996.0292.
55. Ding, L.; Zhang, X.; Zhang, J. Antioxidant Activity In Vitro Guided Screening and Identification of Flavonoids Antioxidants in the Extract from *Tetrastigma hemsleyanum* Diels et Gilg. *Int. J. Anal. Chem.* **2021**, *2021*, 7195125, https://doi.org/10.1155/2021/7195125.
56. Ali, A.; Shah, M.I.A.; Fu, C.; Hussain, Z.; Qureshi, M.N.; Farman, S.; Parveen, Z.; Zada, A.; Nayab, S.; Fazil, P.; Ateeq, M.; Rehman, G.; Naeem, M.; Ibrahim, M.; Khan, M.; Khan, W. Dihydropyrazole

Derivatives Act as Potent α-Amylase Inhibitors and Free Radical Scavengers: Synthesis, Bioactivity Evaluation, Structure–Activity Relationship, ADMET, and Molecular Docking Studies. *ACS Omega* **2023**, *8*, 20412-20422, https://doi.org/10.1021/acsomega.3c00529.

57. Chiu, C.-F.; Lin, Y.-Q.; Park, J.M.; Chen, Y.-C.; Hung, S.-W.; Chiu, C.-C.; Chang, C.-F. The novel camptothecin derivative, CPT211, induces cell cycle arrest and apoptosis in models of human breast cancer. *Biomed. Pharmacother.* **2020**, *128*, 110309, https://doi.org/10.1016/j.biopha.2020.110309.

Publisher's Note & Disclaimer

Supplementary Materials

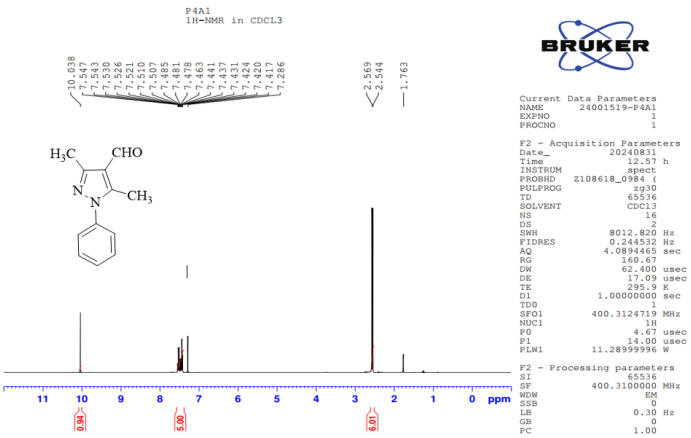

Figure S1. [1]H NMR Spectra of the compound 3,5-Dimethyl-1-phenyl-1*H*-pyrazole-4-carboxaldehyde (**5**).

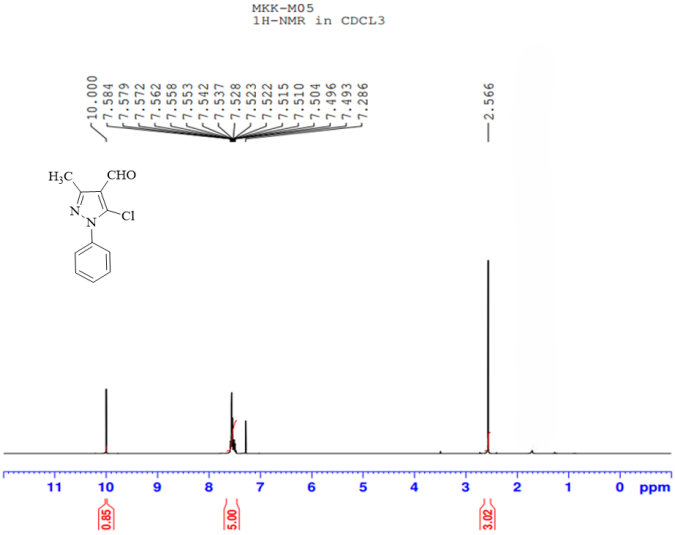

Figure S2. [1]H NMR Spectra of the compound **5-Chloro-3-methyl-1-phenyl-1*H*-pyrazole-4-carbaldehyde (7).**

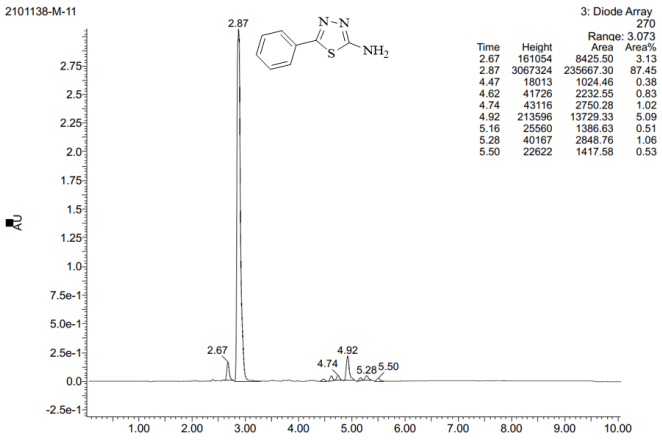

Figure S3. LC Spectra of the compound **5-phenyl-1,3,4-thiadiazol-2-amine (10a).**

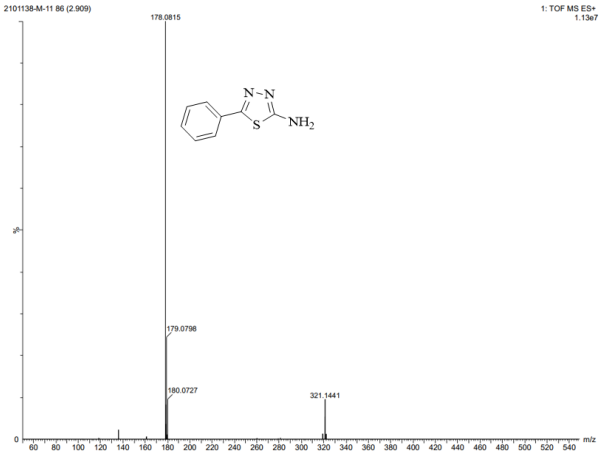

Figure S4. Mass Spectra of the compound **5-phenyl-1,3,4-thiadiazol-2-amine (10a).**

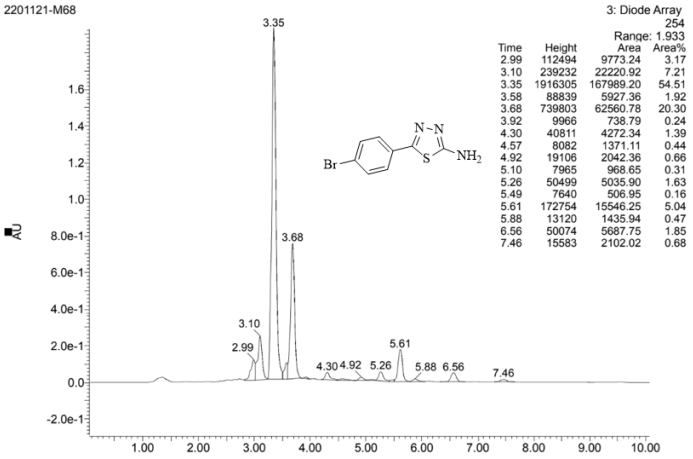

Figure S5. LC Spectra of the compound 5-(4-bromophenyl)-1,3,4-thiadiazol-2-amine (**10b**).

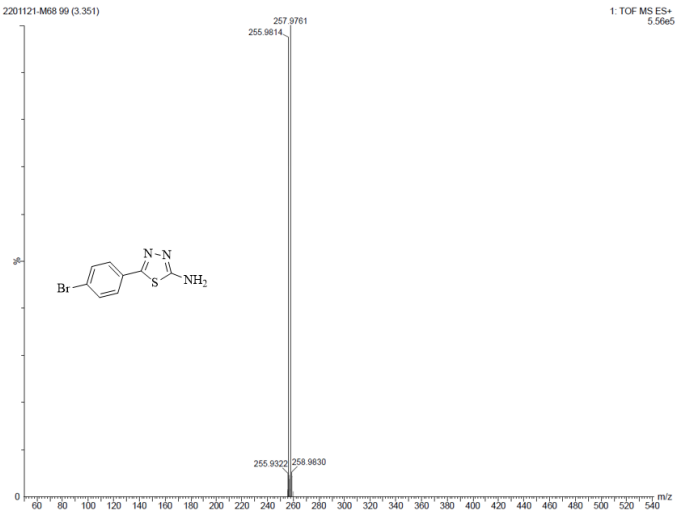

Figure S6. Mass Spectra of the compound 5-(4-bromophenyl)-1,3,4-thiadiazol-2-amine) (**10b**).

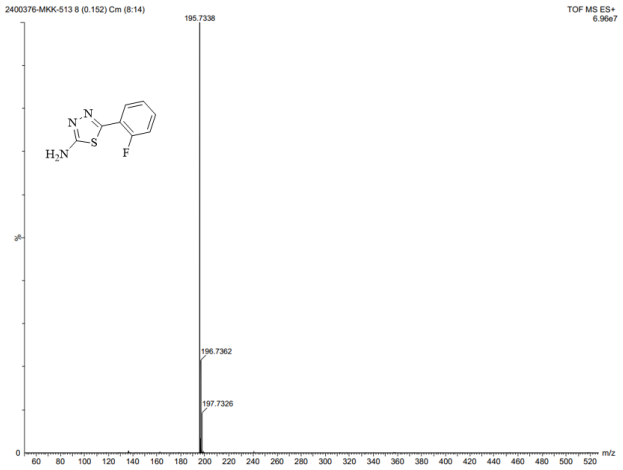

Figure S7. Mass Spectra of the compound 5-(2-fluorophenyl)-1,3,4-thiadiazol-2-amine (**10e**).

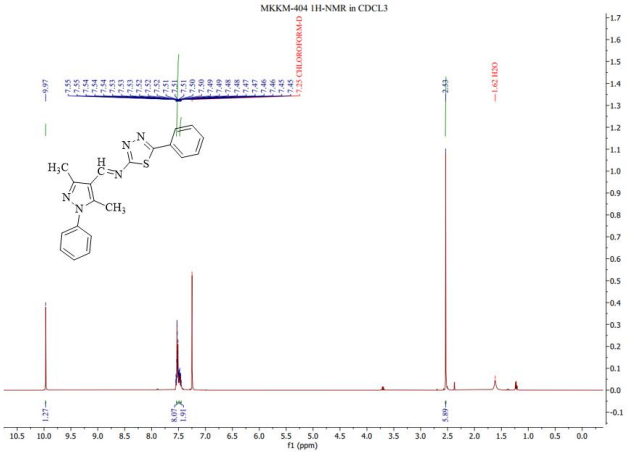

Figure S8. [1]H NMR Spectra of the compound (*E*)-N-((3,5-dimethyl-1-phenyl-1*H*-pyrazol-4-yl)methylene)-5-phenyl-1,3,4-thiadiazol-2-amine (**14a**).

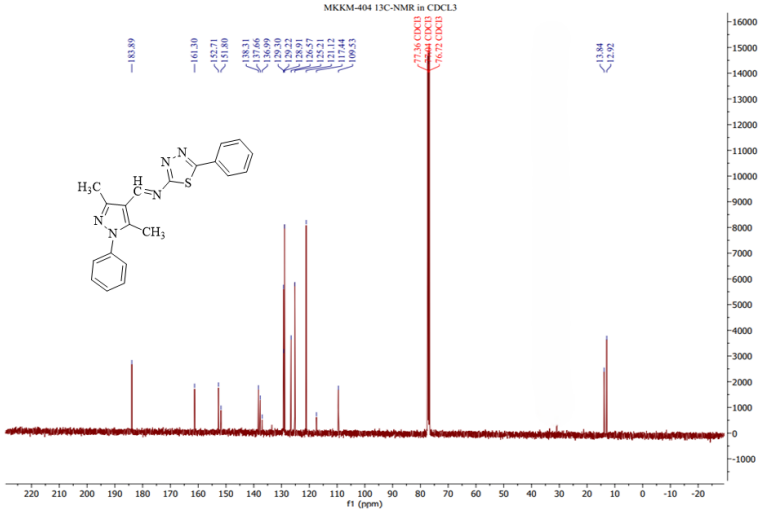

Figure S9. [13]C NMR Spectra of the compound *(E)*-N-((3,5-dimethyl-1-phenyl-1*H*-pyrazol-4-yl)methylene)-5-phenyl-1,3,4-thiadiazol-2-amine (**14a**).

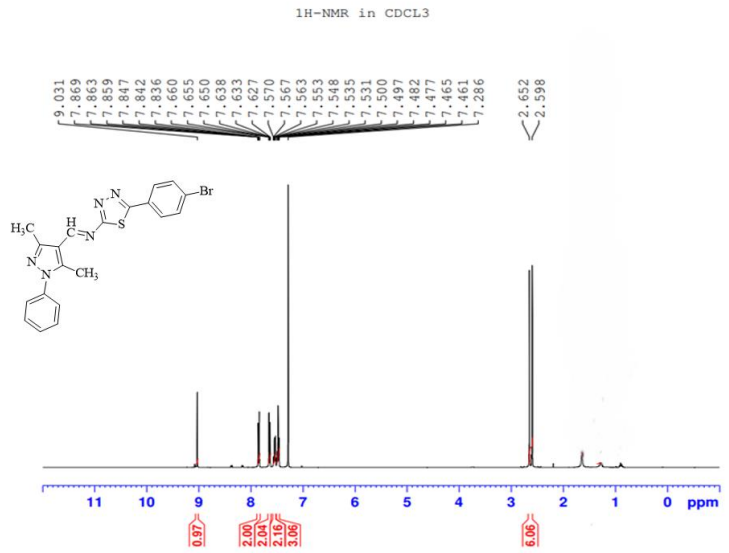

Figure S10. [1]H NMR Spectra of the compound (*E*)-5-(4-bromophenyl)-N-((3,5-dimethyl-1-phenyl-1*H*-pyrazol-4-yl)methylene)-1,3,4-thiadiazol-2-amine (**14b**).

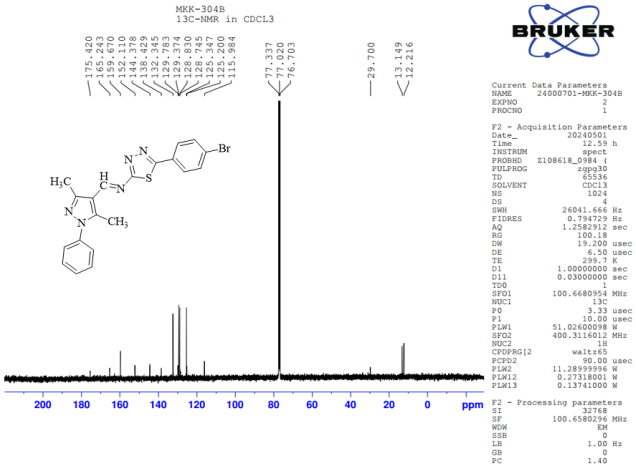

Figure S11. [13]C NMR Spectra of the compound (*E*)-5-(4-bromophenyl)-N-((3,5-dimethyl-1-phenyl-1*H*-pyrazol-4-yl)methylene)-1,3,4-thiadiazol-2-amine (**14b**).

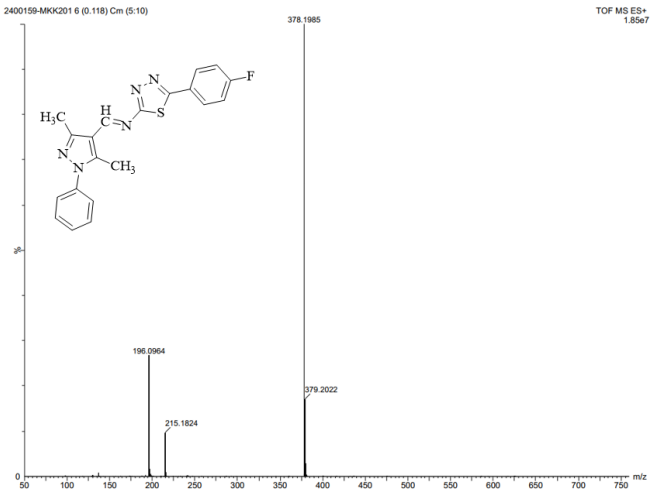

Figure S12. Mass Spectra of the compound (*E*)-N-((3,5-dimethyl-1-phenyl-1*H*-pyrazol-4-yl)methylene)-5-(4-fluorophenyl)-1,3,4-thiadiazol-2-amine **(14c)**

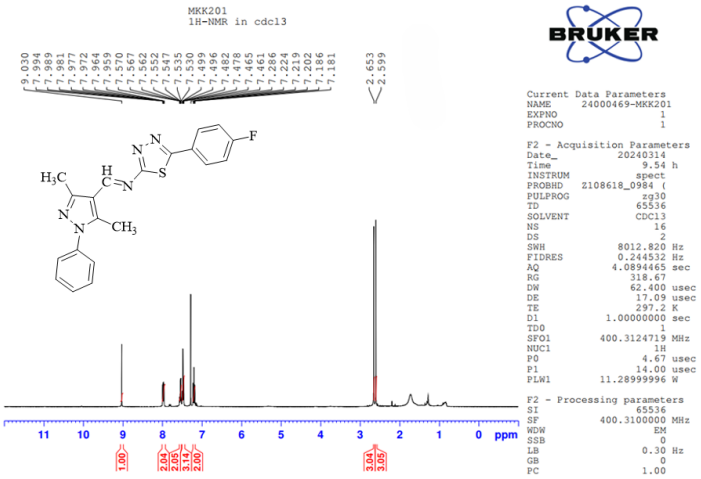

Figure S13. [1]H NMR Spectra of the compound (*E*)-N-((3,5-dimethyl-1-phenyl-1*H*-pyrazol-4-yl)methylene)-5-(4-fluorophenyl)-1,3,4-thiadiazol-2-amine **(14c).**

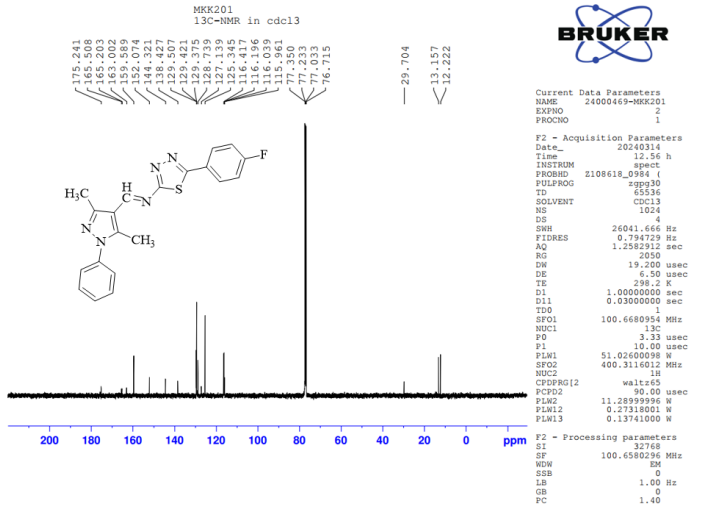

Figure S14. [13]C NMR Spectra of the compound (*E*)-N-((3,5-dimethyl-1-phenyl-1*H*-pyrazol-4-yl)methylene)-5-(4-fluorophenyl)-1,3,4-thiadiazol-2-amine **(14c).**

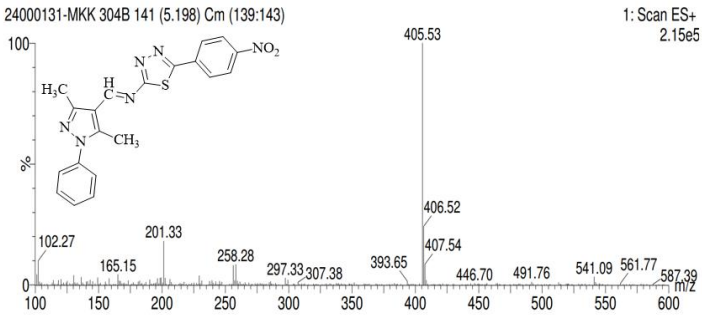

Figure S15. Mass Spectra of the compound (*E*)-N-((3,5-dimethyl-1-phenyl-1*H*-pyrazol-4-yl)methylene)-5-(4-nitrophenyl)-1,3,4-thiadiazol-2-amine (**14d**).

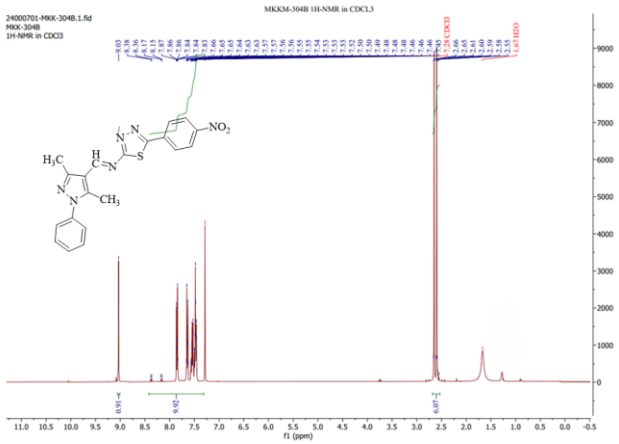

Figure S16. ^{1}H NMR Spectra of the compound (*E*)-N-((3,5-dimethyl-1-phenyl-1*H*-pyrazol-4-yl)methylene)-5-(4-nitrophenyl)-1,3,4-thiadiazol-2-amine (**14d**).

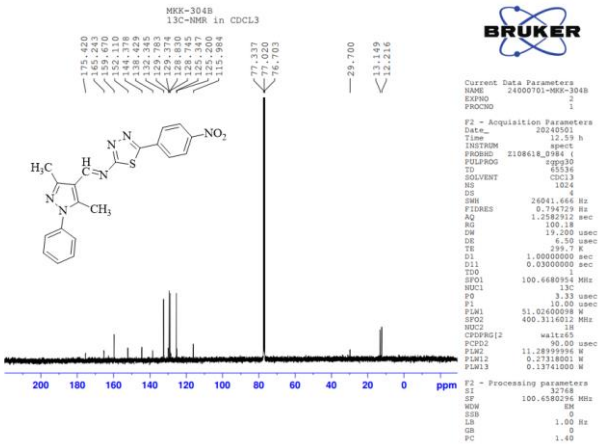

Figure S17. ^{13}C NMR Spectra of the compound (*E*)-N-((3,5-dimethyl-1-phenyl-1*H*-pyrazol-4-yl)methylene)-5-(4-nitrophenyl)-1,3,4-thiadiazol-2-amine (**14d**).

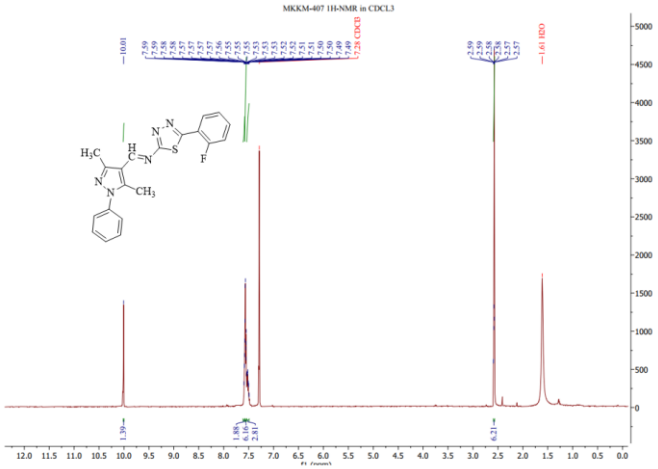

Figure S18. ^{1}H NMR Spectra of the compound (*E*)-N-((3,5-dimethyl-1-phenyl-1*H*-pyrazol-4-yl)methylene)-5-(2-fluorophenyl)-1,3,4-thiadiazol-2-amine (**14e**).

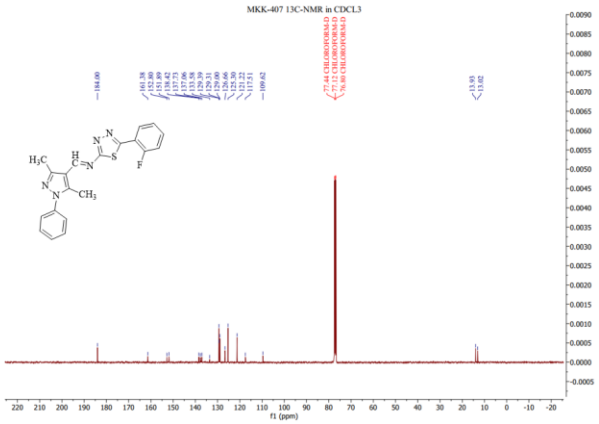

Figure S19. ^{13}C NMR Spectra of the compound (*E*)-N-((3,5-dimethyl-1-phenyl-1*H*-pyrazol-4-yl)methylene)-5-(2-fluorophenyl)-1,3,4-thiadiazol-2-amine (**14e**).

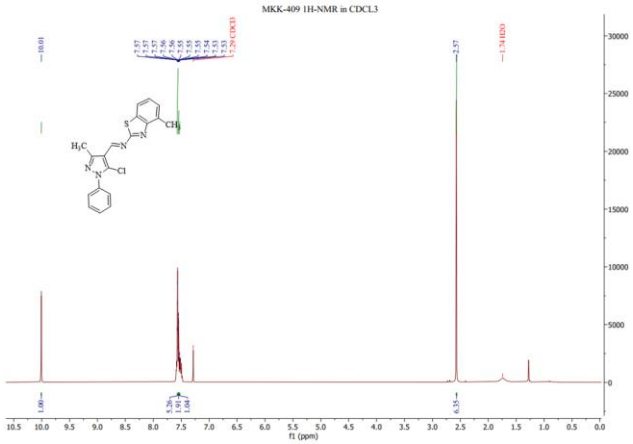

Figure S20. ^{1}H NMR Spectra of the compound (*E*)-N-((5-chloro-3-methyl-1-phenyl-1*H*-pyrazol-4-yl)methylene)-4-methylbenzo[*d*]thiazol-2-amine (**15a**).

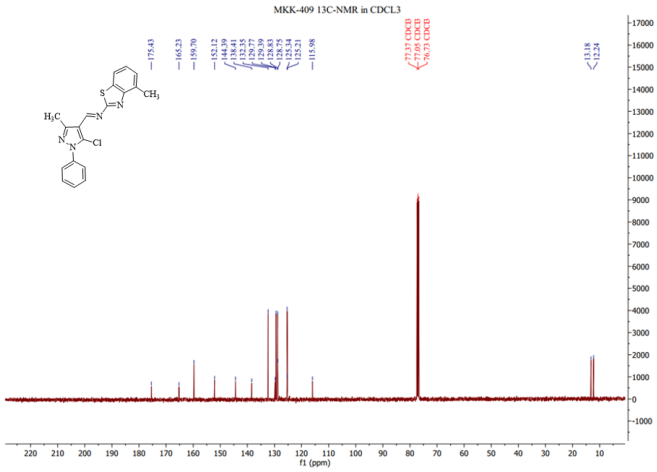

Figure S21. ^{1}H NMR Spectra of the compound (*E*)-N-((5-chloro-3-methyl-1-phenyl-1*H*-pyrazol-4-yl)methylene)-4-methylbenzo[*d*]thiazol-2-amine (**15a**).

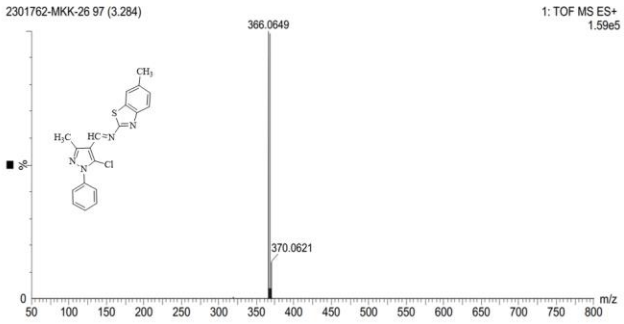

Figure S22. Mass Spectra of the compound (*E*)-N-((5-chloro-3-methyl-1-phenyl-1*H*-pyrazol-4-yl)methylene)-6-methylbenzo[*d*]thiazol-2-amine (**15b**)

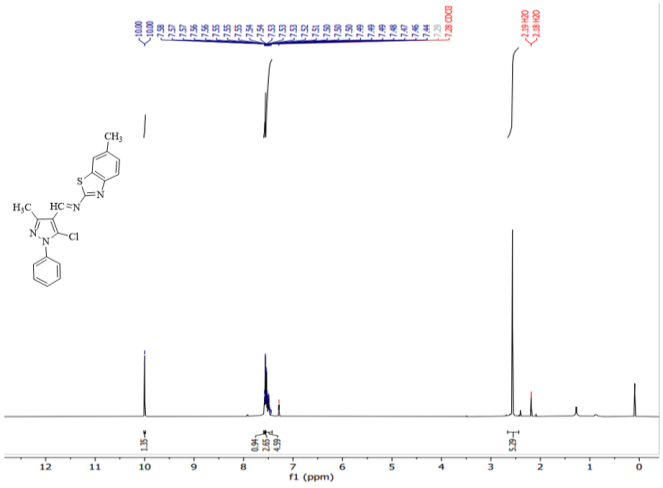

Figure S23. ^{1}H NMR Spectra of the compound (*E*)-N-((5-chloro-3-methyl-1-phenyl-1*H*-pyrazol-4-yl)methylene)-6-methylbenzo[*d*]thiazol-2-amine (**15b**).

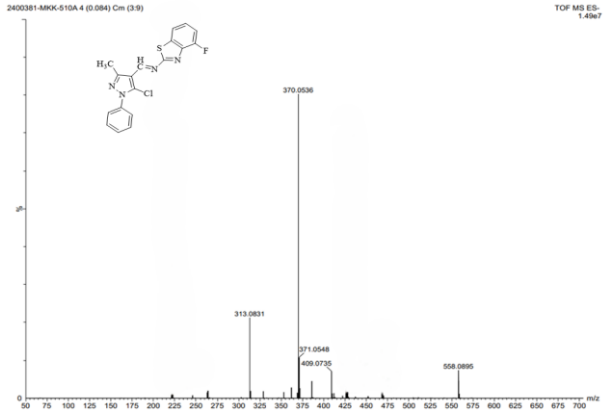

Figure S24. Mass Spectra of the compound (*E*)-N-((5-chloro-3-methyl-1-phenyl-1*H*-pyrazol-4-yl)methylene)-7-fluorobenzo[*d*]thiazol-2-amine **(15c).**

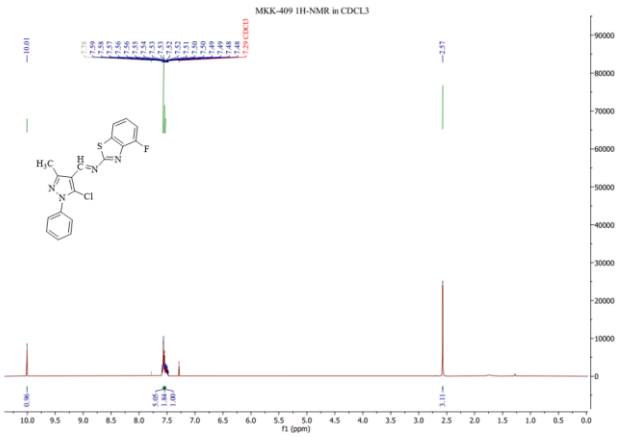

Figure S25. [1]H NMR Spectra of the compound (*E*)-N-((5-chloro-3-methyl-1-phenyl-1*H*-pyrazol-4-yl)methylene)-7-fluorobenzo[*d*]thiazol-2-amine **(15c).**

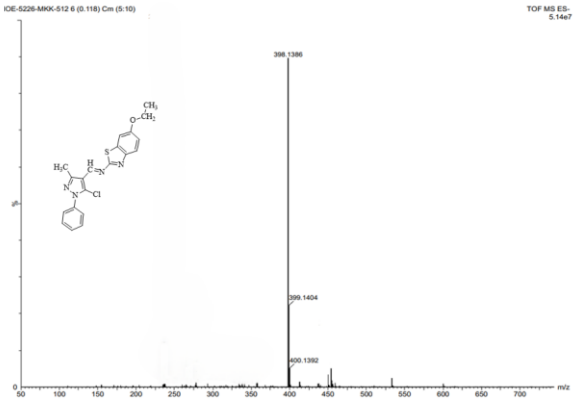

Figure S26. Mass Spectra of the compound (*E*)-N-((5-chloro-3-methyl-1-phenyl-1*H*-pyrazol-4-yl)methylene)-6-ethoxybenzo[*d*]thiazol-2-amine (**15d**).

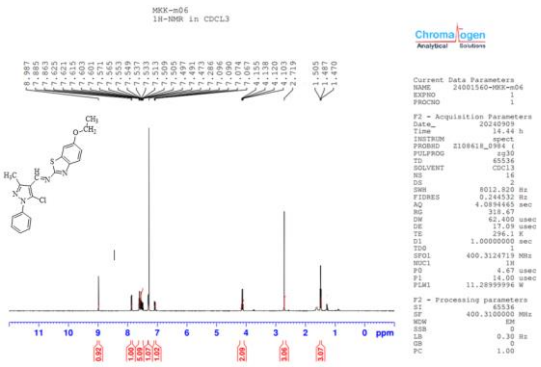

Figure S27. [1]H NMR Spectra of the compound (*E*)-N-((5-chloro-3-methyl-1-phenyl-1*H*-pyrazol-4-yl)methylene)-6-ethoxybenzo[*d*]thiazol-2-amine (**15d**).

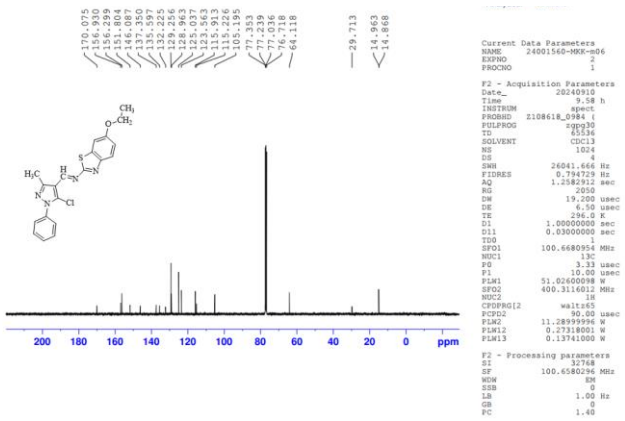

Figure S28. ^{13}C NMR Spectra of the compound (*E*)-N-((5-chloro-3-methyl-1-phenyl-1*H*-pyrazol-4-yl)methylene)-6-ethoxybenzo[*d*]thiazol-2-amine (**15d**).

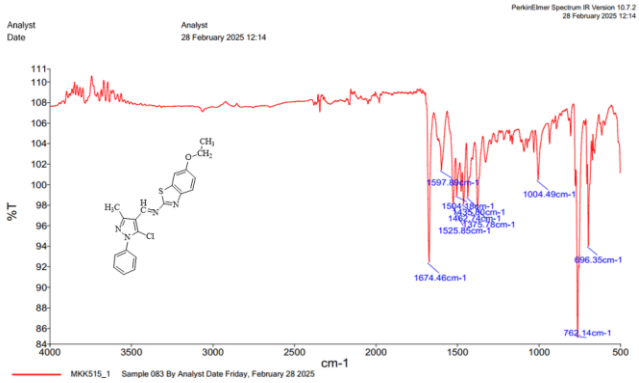

Figure S29. IR Spectra of the compound (*E*)-N-((5-chloro-3-methyl-1-phenyl-1*H*-pyrazol-4-yl)methylene)-6-ethoxybenzo[*d*]thiazol-2-amine (**15d**).

Molecular Docking studies

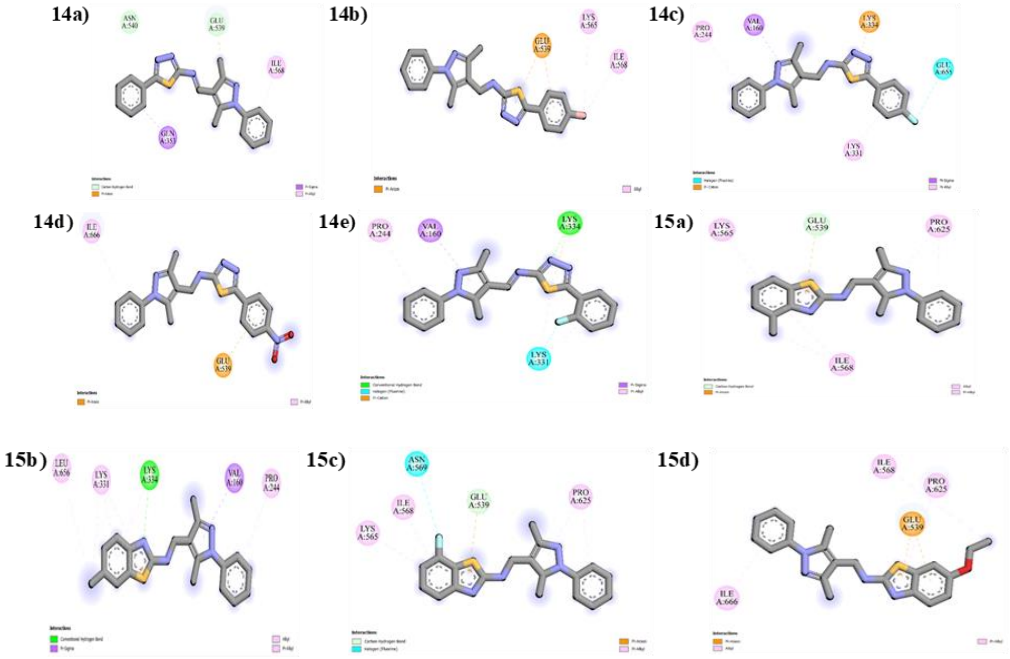

Figure S2.1. Visualization and interpretation of protein-ligand binding forces *via* 2D diagrams (1MWT-ligand interactions).

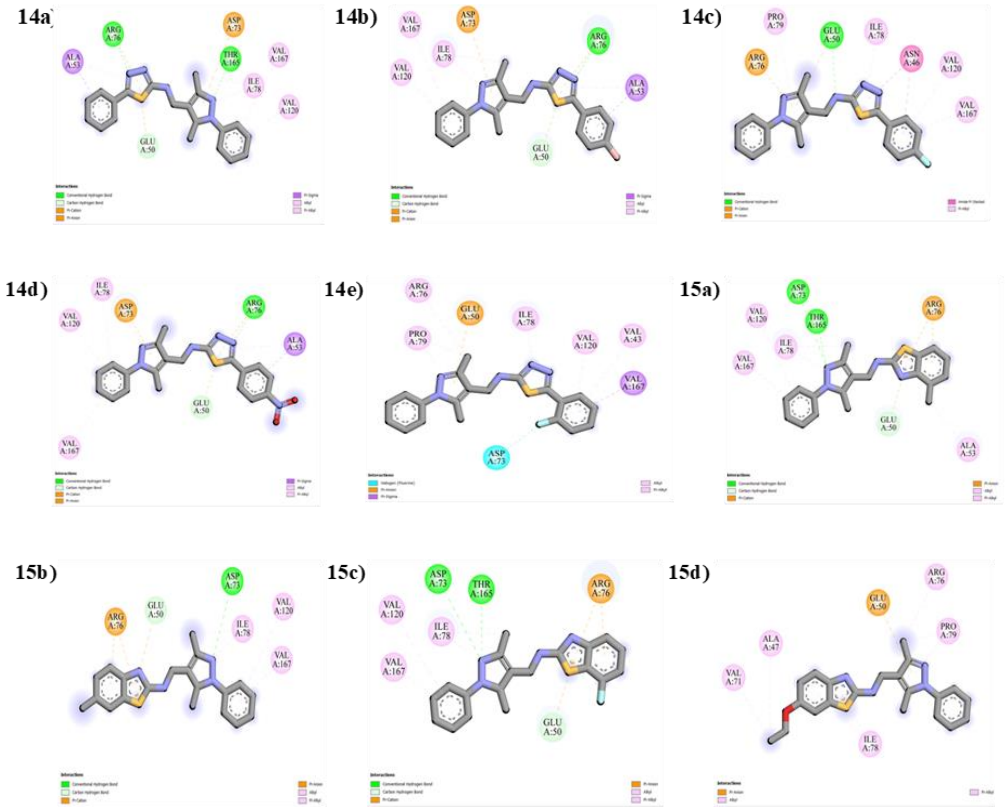

Figure S2.2. Molecular docking 2D interaction of protein (6KZX)-ligand interactions.

Antioxidant activity (DPPH Assay)

Table S3.1. Antioxidant activity of Reference.

Conc of Ascorbic Acid µg/ml	OD 1 @536nm	OD 2 @536nm	Avergae OD	% of Inhibition=AB-AS/AB*100
Blank	0.435	0.44	0.44	0.00
20µg/ml	0.42	0.40	0.41	5.29
40µg/ml	0.231	0.24	0.24	45.98
60µg/ml	0.092	0.09	0.09	79.20
80µg/ml	0.064	0.07	0.07	84.94
100µg/ml	0.059	0.06	0.06	86.90

Table S3.2. Antioxidant activity of (*E*)-N-((3,5-dimethyl-1-phenyl-1*H*-pyrazol-4-yl)methylene)-5-phenyl-1,3,4-thiadiazol-2-amine (**14a**).

Conc. of the compound µg/ml	OD 1 @536nm	OD 2 @536nm	Average OD	% of Inhibition=AB-AS/AB*100
Blank	0.521	0.519	0.52	0.00
20µg/ml	0.442	0.449	0.45	14.33
40µg/ml	0.369	0.365	0.37	29.42
60µg/ml	0.24	0.257	0.25	52.21
80µg/ml	0.215	0.209	0.21	59.23
100µg/ml	0.153	0.156	0.15	70.29

Table S3.3. Antioxidant activity of (*E*)-5-(4-bromophenyl)-N-((3,5-dimethyl-1-phenyl-1*H*-pyrazol-4-yl)methylene)-1,3,4-thiadiazol-2-amine (**14b**).

Conc. of the compound µg/ml	OD 1 @536nm	OD 2 @536nm	Average OD	% of Inhibition=AB-AS/AB*100
Blank	0.521	0.519	0.52	0.00
20µg/ml	0.498	0.495	0.50	4.52
40µg/ml	0.433	0.437	0.44	16.35
60µg/ml	0.41	0.41	0.41	21.15
80µg/ml	0.353	0.348	0.35	32.60
100µg/ml	0.265	0.264	0.26	49.13

Table S3.4. Antioxidant activity of (*E*)-N-((3,5-dimethyl-1-phenyl-1*H*-pyrazol-4-yl)methylene)-5-(4-fluorophenyl)-1,3,4-thiadiazol-2-amine (**14c**).

Conc. of the compound µg/ml	OD 1 @536nm	OD 2 @536nm	Average OD	% of Inhibition=AB-AS/AB*100
Blank	0.521	0.519	0.52	0.00
20µg/ml	0.49	0.472	0.48	7.50
40µg/ml	0.377	0.371	0.37	28.08
60µg/ml	0.338	0.331	0.33	35.67
80µg/ml	0.276	0.278	0.28	46.73
100µg/ml	0.227	0.231	0.23	55.96

Table S3.5. Antioxidant activity of (*E*)-N-((3,5-dimethyl-1-phenyl-1*H*-pyrazol-4-yl)methylene)-5-(4-nitrophenyl)-1,3,4-thiadiazol-2-amine (**14d**).

Conc. of the compound µg/ml	OD 1 @536nm	OD 2 @536nm	Average OD	% of Inhibition=AB-AS/AB*100
Blank	0.521	0.519	0.52	0.00
20µg/ml	0.467	0.469	0.47	10.00
40µg/ml	0.425	0.429	0.43	17.88
60µg/ml	0.385	0.366	0.38	27.79
80µg/ml	0.303	0.319	0.31	40.19
100µg/ml	0.237	0.256	0.25	52.60

Table S3.6. Antioxidant activity of (*E*)-N-((3,5-dimethyl-1-phenyl-1*H*-pyrazol-4-yl)methylene)-5-(2-fluorophenyl)-1,3,4-thiadiazol-2-amine (**14e**).

Conc. of the compound µg/ml	OD 1 @536nm	OD 2 @536nm	Average OD	% of Inhibition=AB-AS/AB*100
Blank	0.521	0.519	0.52	0.00
20µg/ml	0.447	0.435	0.46	11.35
40µg/ml	0.419	0.421	0.43	16.92
60µg/ml	0.344	0.352	0.35	33.08
80µg/ml	0.267	0.252	0.26	50.10
100µg/ml	0.176	0.181	0.18	65.67

Table S3.7. Antioxidant activity of (*E*)-N-((5-chloro-3-methyl-1-phenyl-1*H*-pyrazol-4-yl)methylene)-4-methylbenzo[*d*]thiazol-2-amine (**15a**).

Conc. of the compound µg/ml	OD 1 @536nm	OD 2 @536nm	Average OD	% of Inhibition=AB-AS/AB*100
Blank	0.521	0.519	0.52	0.00
20µg/ml	0.509	0.513	0.51	1.73
40µg/ml	0.462	0.468	0.47	10.58
60µg/ml	0.401	0.412	0.41	21.83
80µg/ml	0.349	0.322	0.34	35.48
100µg/ml	0.285	0.281	0.28	45.58

Table S3.8. Antioxidant activity of (*E*)-N-((5-chloro-3-methyl-1-phenyl-1*H*-pyrazol-4-yl)methylene)-6-methylbenzo[*d*]thiazol-2-amine (**15b**).

Conc. of the compound µg/ml	OD 1 @536nm	OD 2 @536nm	Average OD	% of Inhibition=AB-AS/AB*100
Blank	0.521	0.519	0.52	0.00
20µg/ml	0.508	0.509	0.51	2.21
40µg/ml	0.466	0.467	0.47	10.29
60µg/ml	0.411	0.415	0.41	20.58
80µg/ml	0.351	0.355	0.35	32.12
100µg/ml	0.293	0.298	0.30	43.17

Table S3.9. Antioxidant activity of (*E*)-N-((5-chloro-3-methyl-1-phenyl-1*H*-pyrazol-4-yl)methylene)-7-fluorobenzo[*d*]thiazol-2-amine (**15c**).

Conc. of the compound µg/ml	OD 1 @536nm	OD 2 @536nm	Average OD	% of Inhibition=AB-AS/AB*100
Blank	0.521	0.519	0.52	0.00
20µg/ml	0.505	0.503	0.50	3.08
40µg/ml	0.459	0.455	0.46	12.12
60µg/ml	0.389	0.385	0.39	25.58
80µg/ml	0.322	0.324	0.32	37.88
100µg/ml	0.275	0.258	0.27	48.75

Table S3.10. Antioxidant activity of (*E*)-N-((5-chloro-3-methyl-1-phenyl-1*H*-pyrazol-4-yl)methylene)-6-ethoxybenzo[*d*]thiazol-2-amine (**15d**).

Conc. of the compound µg/ml	OD 1 @536nm	OD 2 @536nm	Average OD	% of Inhibition=AB-AS/AB*100
Blank	0.521	0.519	0.52	0.00
20µg/ml	0.473	0.481	0.48	8.27
40µg/ml	0.366	0.369	0.37	29.33
60µg/ml	0.338	0.325	0.33	36.25
80µg/ml	0.266	0.273	0.27	48.17
100µg/ml	0.226	0.232	0.23	55.96

Antioxidant activity (FRAP assay)

Table S4.1. FRAP Assay of Reference.

Concentration of ferric sulphate µM	OD1 @ 593nm	OD2 @593nm	Average OD	Net OD
0	0.095	0.1	0.0975	0.00
1600	1.18	1.188	1.184	1.09
1400	1.047	1.116	1.0815	0.98
1200	0.93	1	0.965	0.87
1000	0.786	0.76	0.773	0.68
800	0.698	0.697	0.6975	0.60
600	0.48	0.5	0.49	0.39
400	0.383	0.368	0.3755	0.28
200	0.249	0.242	0.2455	0.15

Table S4.2. FRAP Assay of (*E*)-N-((3,5-dimethyl-1-phenyl-1*H*-pyrazol-4-yl)methylene)-5-phenyl-1,3,4-thiadiazol-2-amine (**14a**).

Conc. of the compound µg/ml	OD1 @ 593nm	OD2 @593nm	Average OD	Net OD
Blank	0.095	0.1	0.0975	0.00
20µg/ml	1.094	1.021	1.0575	0.96
40µg/ml	0.782	0.785	0.7835	0.69
60µg/ml	0.657	0.672	0.6645	0.57
80µg/ml	0.596	0.615	0.6055	0.51
100µg/ml	0.422	0.441	0.4315	0.33

Table S4.3. FRAP Assay of (*E*)-N-((3,5-dimethyl-1-phenyl-1*H*-pyrazol-4-yl)methylene)-5-(4-fluorophenyl)-1,3,4-thiadiazol-2-amine (**14c**).

Conc. of the compound µg/ml	OD1 @ 593nm	OD2 @593nm	Average OD	Net OD
Blank	0.095	0.1	0.0975	0.00
20µg/ml	1.231	1.113	1.172	1.07
40µg/ml	0.832	0.845	0.8385	0.74
60µg/ml	0.717	0.705	0.711	0.61
80µg/ml	0.618	0.612	0.615	0.52
100µg/ml	0.482	0.455	0.468	0.37

Table S4.4. FRAP Assay of (*E*)-N-((3,5-dimethyl-1-phenyl-1*H*-pyrazol-4-yl)methylene)-5-(4-nitrophenyl)-1,3,4-thiadiazol-2-amine (**14d**).

Conc. of the compound µg/ml	OD1 @ 593nm	OD2 @593nm	Average OD	Net OD
Blank	0.095	0.1	0.0975	0.00
20µg/ml	0.973	0.978	0.9755	0.88
40µg/ml	0.745	0.763	0.754	0.66
60µg/ml	0.612	0.687	0.6495	0.55
80µg/ml	0.565	0.582	0.5735	0.48
100µg/ml	0.403	0.408	0.4055	0.31

Table S4.5. FRAP Assay of (*E*)-N-((3,5-dimethyl-1-phenyl-1*H*-pyrazol-4-yl)methylene)-5-(2-fluorophenyl)-1,3,4-thiadiazol-2-amine (**14e**).

Conc. of the compound µg/ml	OD1 @ 593nm	OD2 @593nm	Average OD	Net OD
Blank	0.095	0.1	0.0975	0.00
20µg/ml	1.142	1.39	1.266	1.17
40µg/ml	0.867	0.875	0.871	0.77
60µg/ml	0.724	0.749	0.7365	0.64
80µg/ml	0.645	0.658	0.6515	0.55
100µg/ml	0.547	0.568	0.5575	0.46

Table S4.7. FRAP Assay of (*E*)-N-((5-chloro-3-methyl-1-phenyl-1*H*-pyrazol-4-yl)methylene)-7-fluorobenzo[*d*]thiazol-2-amine) (**15c**).

Conc. of the compound µg/ml	OD1 @ 593nm	OD2 @593nm	Average OD	Net OD
Blank	0.095	0.1	0.0975	0.00
20µg/ml	0.897	0.911	0.904	0.81
40µg/ml	0.711	0.729	0.72	0.62
60µg/ml	0.619	0.615	0.617	0.52
80µg/ml	0.522	0.527	0.5245	0.43
100µg/ml	0.378	0.39	0.384	0.29

Table S4.8. FRAP Assay of (*E*)-N-((5-chloro-3-methyl-1-phenyl-1*H*-pyrazol-4-yl)methylene)-6-ethoxybenzo[*d*]thiazol-2-amine (**15d**).

Conc. of the compound µg/ml	OD1 @ 593nm	OD2 @593nm	Average OD	Net OD
Blank	0.095	0.1	0.0975	0.00
20µg/ml	0.819	0.836	0.8275	0.73
40µg/ml	0.644	0.652	0.648	0.55
60µg/ml	0.513	0.551	0.532	0.43
80µg/ml	0.457	0.464	0.4605	0.36
100µg/ml	0.351	0.335	0.343	0.25